Dioxygen Binding to Complexes with Fe$^{II}_2$(μ-OH)$_2$ Cores: Steric Control of Activation Barriers and O$_2$-Adduct Formation

Sergey V. Kryatov, Sonia Taktak, Ivan V. Korendovych, and Elena V. Rybak-Akimova*

Department of Chemistry, Tufts University, 62 Talbot Avenue, Medford, Massachusetts 02155

József Kaizer, Stéphane Torelli, Xiaopeng Shan, Sanjay Mandal, Vicki L. MacMurdo, Antoni Mairata i Payeras, and Lawrence Que, Jr.*

Department of Chemistry and Center for Metals in Biocatalysis, University of Minnesota, 207 Pleasant Street SE, Minneapolis, Minnesota 55455

A series of complexes with [Fe$^{II}_2$(μ-OH)$_2$] cores has been synthesized with N3 and N4 ligands and structurally characterized to serve as models for nonheme diiron(II) sites in enzymes that bind and activate O$_2$. These complexes react with O$_2$ in solution via bimolecular rate-limiting steps that differ in rate by 10^3-fold, depending on ligand denticity and steric hindrance near the diiron center. Low-temperature trapping of a (μ-oxo)(μ-1,2-peroxo)diiron(III) intermediate after O$_2$ binding requires sufficient steric hindrance around the diiron center and the loss of a proton (presumably that of a hydroxo bridge or a yet unobserved hydroperoxo intermediate). The relative stability of these and other (μ-1,2-peroxo)diiron(III) intermediates suggests that these species may not be on the direct pathway for dioxygen activation.

Introduction

Diiron(II) centers participate in the binding and activation of dioxygen at a number of metalloprotein active sites.[1–3] The reactions that occur include reversible oxygenation of hemerythrin[4] and the oxidations of various substrates, such as the formation of a catalytically essential tyrosyl radical from an endogenous tyrosine in class I ribonucleotide reductases (RNR),[5] the dehydrogenation of fatty acid alkyl chains by stearoyl-ACP Δ^9-desaturase (Δ9D),[6] and the hydroxylation of methane and alkanes by soluble methane monooxygenase (M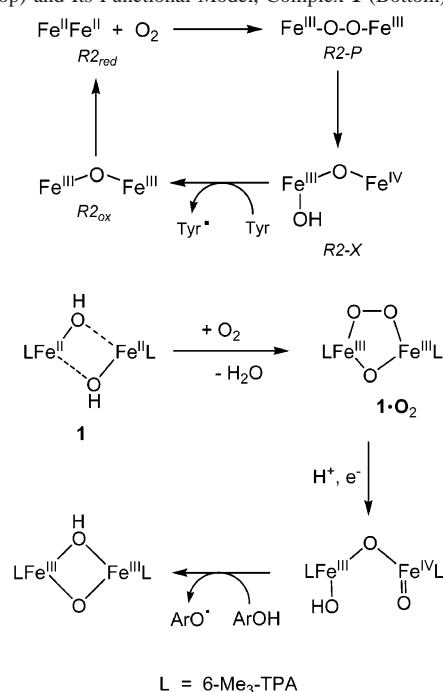MO)[7] and membrane bound alkane monooxy-genases.[8] Extensive studies have identified diiron(III)–peroxo and higher-valent iron–oxo intermediates in the catalytic cycles of some of these enzymes. A terminal end-on hydroperoxide is established for oxyhemerythrin,[4] while bridged peroxo species are observed for MMO,[1,7] Δ9D,[9] and a mutant RNR.[10] An iron(III)iron(IV) intermediate called X is directly responsible for tyrosyl radical formation in RNR,[5] while a diiron(IV) intermediate called Q is the key oxidant that hydroxylates methane in MMO.[1,7]

Model complexes have played critical roles in providing synthetic precedents for the proposed structures of these catalytic intermediates.[3,11–15] For the peroxo intermediates that are the focus of this paper, several O$_2$ adducts of
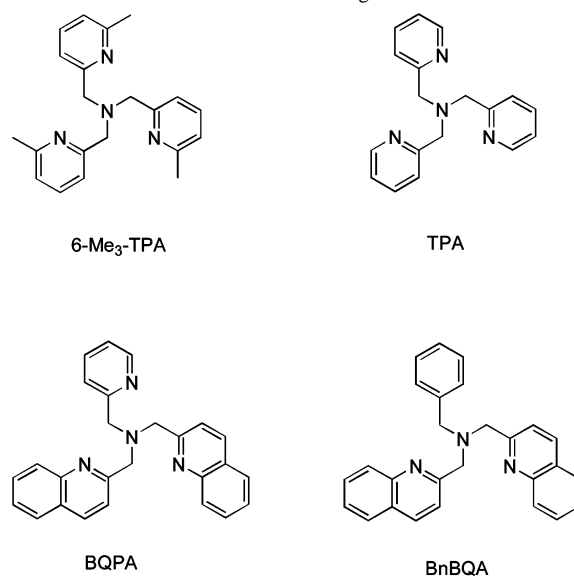
* To whom correspondence should be addressed. E-mail: elena.rybak-akimova@tufts.edu (E.V.R.-A.); que@chem.umn.edu (L.Q.).
(1) Wallar, B. J.; Lipscomb, J. D. *Chem. Rev.* **1996**, *96*, 2625–2657.
(2) Solomon, E. I.; Brunold, T. C.; Davis, M. I.; Kemsley, J. N.; Lee, S.-K.; Lehnert, N.; Neese, F.; Skulan, A. J.; Yang, Y.-S.; Zhou, J. *Chem. Rev.* **2000**, *100*, 235–349.
(3) Lee, D.; Lippard, S. J. Nonheme Di-iron Enzymes. In *Comprehensive Coordination Chemistry II*; McCleverty, J. A., Meyer, T. J., Eds.; Elsevier: Oxford, U.K., 2004; Vol. 8, pp 309–342.
(4) Stenkamp, R. E. *Chem. Rev.* **1994**, *94*, 715–726.
(5) Stubbe, J.; Riggs-Gelasco, P. *Trends Biochem. Sci.* **1998**, *23*, 438–443.
(6) Broadwater, J. A.; Haas, J. A.; Fox, B. G. *Fett/Lipid* **1998**, *100*, 103–113.
(7) Merkx, M.; Kopp, D. A.; Sazinsky, M. H.; Blazyk, J. L.; Müller, J.; Lippard, S. J. *Angew. Chem., Int. Ed.* **2001**, *40*, 2782–2807.
(8) Shanklin, J.; Whittle, E. *FEBS Lett.* **2003**, *545*, 188–192.
(9) Broadwater, J. A.; Ai, J.; Loehr, T. M.; Sanders-Loehr, J.; Fox, B. G. *Biochemistry* **1998**, *37*, 14664–14671.
(10) Moënne-Loccoz, P.; Baldwin, J.; Ley, B. A.; Loehr, T. M.; Bollinger, J. M., Jr. *Biochemistry* **1998**, *37*, 14659–14663.
(11) Que, L., Jr.; Dong, Y. *Acc. Chem. Res.* **1996**, *29*, 190–196.
(12) Que, L., Jr.; Tolman, W. B. *Angew. Chem., Int. Ed.* **2002**, *41*, 1114–1137.
(13) Suzuki, M.; Furutachi, H.; Okawa, H. *Coord. Chem. Rev.* **2000**, *200–202*, 105–129.
(14) Du Bois, J.; Mizoguchi, T. J.; Lippard, S. J. *Coord. Chem. Rev.* **2000**, *200–202*, 443–485.
(15) Tolman, W. B.; Que, L., Jr. *J. Chem. Soc., Dalton Trans.* **2002**, 653–660.

Scheme 1. Catalytic Cycle of the Diiron Center in the R2 RNR Protein (Top) and Its Functional Model, Complex **1** (Bottom)

L = 6-Me$_3$-TPA

Scheme 2. Structural Formulas of the Ligands Used in This Work

6-Me$_3$-TPA

TPA

BQPA

BnBQA

diiron(II) complexes have been characterized.[3,13−29] Efforts in the mid-1990s led to the crystallization of three O$_2$ adducts whose structures revealed the formation of (μ-1,2-peroxo)-diiron(III) units supported by additional alkoxo and/or carboxylate bridges.[16,18,19] For these examples, the peroxo intermediate was either quite stable or underwent subsequent decay to iron(III) products without evidence of any higher-valent iron species that may result from O−O bond cleavage. Subsequently, the diiron(II) complex [Fe$_2$(μ-OH)$_2$(6-Me$_3$-

TPA)$_2$]$^{2+}$ (**1**) was synthesized and structurally characterized.[26] This complex reacted with O$_2$ at low temperature to generate a metastable peroxo intermediate, which could undergo an acid-promoted conversion to an Fe(III)Fe(IV) species capable of oxidizing phenols.[26] This system thus mimics all essential steps in the formation of the diiron(III)−tyrosyl radical cofactor of RNR (Scheme 1).[12,26] However, for **1**, the rates of the individual reactions shown in Scheme 1 are substantially slower than those of the corresponding enzymatic transformations.[26,27] Detailed studies of the oxygenation of this complex suggested that the steric bulk imposed by the 6-methyl substituents on the pyridines shielded the diiron site from access by O$_2$.[27] We anticipated that removing methyl substituents and/or replacing CH$_3$ groups with planar aromatic substituents would significantly influence the accessibility of the iron centers and the rates of key reactions in O$_2$ activation cycle. We have thus introduced systematic changes in the ligand structure (Scheme 2) to prepare a series of complexes with [Fe$^{II}_2$(μ-OH)$_2$] cores. These complexes react with O$_2$ at rates that differ by 10^3-fold. Detailed structural characterization of this series of complexes and electrochemical studies of their redox properties allow us to evaluate the relative importance of steric and electronic factors in the oxygenation kinetics. This first detailed study of a series of [Fe$^{II}_2$(μ-OH)$_2$] complexes re-emphasizes the importance of steric control and coordinative unsaturation in facilitating O$_2$ attack at a diiron center and points out a requirement for the loss of a proton after initial adduct formation in order for the (μ-1,2-peroxo)diiron(III) adduct to be trapped.

Experimental Section

Syntheses. Ligands TPA, 6-Me$_3$-TPA, and BQPA (Scheme 2) were synthesized according to literature methods.[30−32] Commercially available chemicals were purchased and used without further

(16) Ookubo, T.; Sugimoto, H.; Nagayama, T.; Masuda, H.; Sato, T.; Tanaka, K.; Maeda, Y.; Okawa, H.; Hayashi, Y.; Uehara, A.; Suzuki, M. *J. Am. Chem. Soc.* **1996**, *118*, 701−702.
(17) Sugimoto, H.; Nagayama, T.; Maruyama, S.; Fujinami, S.; Yasuda, Y.; Suzuki, M.; Uehara, A. *Bull. Chem. Soc. Jpn.* **1998**, *71*, 2267−2279.
(18) Kim, K.; Lippard, S. J. *J. Am. Chem. Soc.* **1996**, *118*, 4914−4915.
(19) Dong, Y.; Yan, S.; Young, V. G., Jr.; Que, L., Jr. *Angew. Chem., Int. Ed. Engl.* **1996**, *35*, 618−620.
(20) Kitajima, N.; Tamura, N.; Amagai, H.; Fukui, H.; Moro-oka, Y.; Mizutani, Y.; Kitagawa, T.; Mathur, R.; Heerwegh, K.; Reed, C. A.; Randall, C. R.; Que, L., Jr.; Tatsumi, K. *J. Am. Chem. Soc.* **1994**, *116*, 9071−9085.
(21) Hayashi, Y.; Kayatani, T.; Sugimoto, H.; Suzuki, M.; Inomata, K.; Uehara, A.; Muzitani, Y.; Kitagawa, T.; Maeda, Y. *J. Am. Chem. Soc.* **1995**, *117*, 11220−11229.
(22) (a) Feig, A. L.; Becker, M.; Schindler, S.; van Eldik, R.; Lippard, S. J. *Inorg. Chem.* **1996**, *35*, 2590−2601. (b) Feig, A. L.; Becker, M.; Schindler, S.; van Eldik, R.; Lippard, S. J. *Inorg. Chem.* **2003**, *42*, 3704.
(23) Herold, S.; Lippard, S. J. *J. Am. Chem. Soc.* **1997**, *119*, 145−156.
(24) LeCloux, D. D.; Barrios, A. M.; Lippard, S. J. *Bioorg. Med. Chem.* **1999**, *7*, 763−772.
(25) Mizoguchi, T. J.; Kuzelka, J.; Spingler, B.; DuBois, J. L.; Davydov, R. M.; Hedman, B.; Hodgson, K. O.; Lippard, S. J. *Inorg. Chem.* **2001**, *40*, 4662−4673.
(26) MacMurdo, V. L.; Zheng, H.; Que, L., Jr. *Inorg. Chem.* **2000**, *39*, 2254−2255.
(27) Kryatov, S. V.; Rybak-Akimova, E. V.; MacMurdo, V. L.; Que, L., Jr. *Inorg. Chem.* **2001**, *40*, 2220−2228.
(28) Costas, M.; Cady, C. W.; Kryatov, S. V.; Ray, M.; Ryan, M. J.; Rybak-Akimova, E. V.; Que, L., Jr. *Inorg. Chem.* **2003**, *42*, 7519−7530.
(29) Kryatov, S. V.; Chavez, F. A.; Reynolds, A. M.; Rybak-Akimova, E. V.; Que, L., Jr.; Tolman, W. B. *Inorg. Chem.* **2004**, *43*, 2141−2150.

(30) Tyeklar, Z.; Jacobson, R. R.; Wei, N.; Murthy, N. N.; Zubieta, J.; Karlin, K. D. *J. Am. Chem. Soc.* **1993**, *115*, 2677−2689.
(31) Da Mota, M. M.; Rodgers, J.; Nelson, S. M. *J. Chem. Soc. A* **1969**, 2036−2044.

purification. Syntheses and manipulation of iron(II) complexes were conducted in a glovebox under inert atmosphere. Elemental analyses were performed at MHW Laboratories (Phoenix, AZ). *Caution: Perchlorate salts are potentially explosive and should be handled with care!*

N-Benzyl-N,N-di(quinolin-2-ylmethyl)amine, BnBQA. 2-Chloromethylquinoline hydrochloride (3.64 g, 17 mmol), benzyl-amine (0.86 g, 8.02 mmol), and Na$_2$CO$_3$ (24 g, 280 mmol) dissolved in water (20 mL) were combined in 200 mL of CH$_3$CN. The resulting suspension was heated to reflux for 30 h. The mixture was then filtered, and the filtrate was reduced in volume. After addition of 30 mL of water to the concentrated filtrate, the product was extracted by CH$_2$Cl$_2$ (3 × 50 mL) and dried over Na$_2$SO$_4$. The filtrate was evaporated to yield a yellow oil, to which Et$_2$O was added. Partial evaporation of the solvent resulted in precipitation of the title compound as yellow crystals (2.3 g, 74%). ^{1}H NMR (CDCl$_3$): δ (ppm) 8.15 (2H, d), 8.07 (2H, d), 7.79 (2H, m), 7.77 (2H, d), 7.70 (2H, m), 7.52 (2H, m), 7.47 (2H, d), 7.34 (2H, m), 7.24 (1H, m), 4.03 (4H, s), 3.78 (2H, s).

[Fe$_2$(μ-OH)$_2$(6-Me$_3$-TPA)$_2$](CF$_3$SO$_3$)$_2$, 1(OTf)$_2$, was synthesized by a procedure analogous to that published elsewhere for **1**(ClO$_4$)$_2$.[26] The anaerobic reaction of equimolar amounts of Fe(OTf)$_2$·2CH$_3$CN, 6-Me$_3$-TPA, and NaOH in methanol, followed by recrystallization of the crude complex from CH$_3$CN/diethyl ether at 4 °C, afforded **1**(OTf)$_2$ as an orange solid in 56% yield. Solid **1**(OTf)$_2$ is stable under inert atmosphere at room temperature. UV−vis (CH$_3$CN): λ_{max}, nm (ε, M^{-1} cm^{-1}), 420 (2400). Anal. Calcd for **1**(OTf)$_2$·2CH$_3$CN or C$_{48}$H$_{56}$F$_6$Fe$_2$N$_{10}$O$_8$S$_2$ (Found): C, 48.41 (48.57); H, 4.74 (4.87); N, 11.76 (11.59).

[Fe$_2$(μ-OH)$_2$(TPA)$_2$](ClO$_4$)$_2$, 2(ClO$_4$)$_2$. Equimolar amounts of Fe(ClO$_4$)$_2$·6H$_2$O (0.36 g, 1.0 mmol) and TPA (0.29 g, 1 mmol) were mixed together in degassed methanol (10 mL), forming a yellow solution. Addition of 1 equiv of solid NaOH (0.040 g, 1 mmol) formed a red solution. Complex **2**(ClO$_4$)$_2$ could then be crystallized as a dark-red solid from the solution by layering with Et$_2$O. Anal. Calcd for **2**(ClO$_4$)$_2$ or C$_{36}$H$_{38}$Cl$_2$Fe$_2$N$_8$O$_{10}$ (Found): C, 46.73 (46.49); H, 4.14 (4.04); N, 12.11 (11.86); Cl, 7.66 (7.94). UV−vis (CH$_3$CN): λ_{max}, nm (ε, M^{-1} cm^{-1}), 465 (2800).

[Fe$_2$(μ-OH)$_2$(TPA)$_2$](CF$_3$SO$_3$)$_2$, 2(OTf)$_2$. This compound was prepared as a dark-red solid following the method for **2**(ClO$_4$)$_2$ and substituting Fe(ClO$_4$)$_2$·6H$_2$O for an equivalent amount of Fe(OTf)$_2$·2CH$_3$CN and 6 equiv of H$_2$O. Yield: 57%. Crystals suitable for the X-ray analysis formed directly from the reaction mixture. Anal. Calcd for **2**(OTf)$_2$, C$_{38}$H$_{38}$F$_6$Fe$_2$N$_8$O$_8$S$_2$ (Found): C, 44.55 (44.31); H, 3.74 (4.09); N, 10.94 (10.82). UV−vis (CH$_3$CN): λ_{max}, nm (ε, M^{-1} cm^{-1}), 465 (2800). Due to its better solubility, the triflate salt **2**(OTf)$_2$ was used for the kinetic investigation. Solids **2**(ClO$_4$)$_2$ and **2**(OTf)$_2$ slowly decompose at room temperature even under inert atmosphere and should be kept in a freezer.

[Fe$_2$(μ-OH)$_2$(BQPA)$_2$](CF$_3$SO$_3$)$_2$, 3(OTf)$_2$. To a solution of BQPA (0.15 g, 0.385 mmol) in methanol (10 mL) under argon was added dropwise Fe(OTf)$_2$·2CH$_3$CN (0.17 g, 0.385 mmol) in methanol (5 mL). The yellow orange solution immediately turned red. NaOH (1 equiv, 0.016 g, 0.39 mmol) was then added as solid (or as a solution in methanol), and the color changed to dark red. After stirring overnight, the solvent was removed under vacuum. The resulting dark red-brown solid was dissolved in CH$_2$Cl$_2$, and the solution was filtered to remove insoluble impurities. The solvent was removed again, and the red brown powder that was obtained was dried under vacuum. Recrystallization from CH$_3$CN/ether

afforded brown crystals suitable for X-ray diffraction. Solid **3**(OTf)$_2$ is stable under inert atmosphere at room temperature for a long time. Anal. Calcd for **3**(OTf)$_2$·2CH$_3$CN or C$_{58}$H$_{52}$F$_6$Fe$_2$N$_{10}$O$_8$S$_2$ (Found): C, 53.30 (53.55); H, 4.01 (4.12); N, 10.72 (10.58). UV−vis (CH$_3$CN): λ_{max}, nm (ε, M^{-1} cm^{-1}), 445 (2900), 550 (2100).

[Fe$_2$(μ-OH)$_2$(BnBQA)$_2$(CH$_3$CN)$_2$](ClO$_4$)$_2$, 4(ClO$_4$)$_2$. To a solution of BnBQA (0.39 g, 1.0 mM) in CH$_3$CN (3 mL) under argon was added a solution of Fe(ClO$_4$)$_2$·6H$_2$O (0.36 g, 1.0 mM) in CH$_3$CN (2 mL) dropwise. The yellow-orange solution immediately turned dark red. NEt$_3$ (1 equiv, 1 mM, 130 μL) was then added, and the color changed to dark red-purple. The solution was stirred for 2 h, layered with ether (5 mL), and left for crystallization to yield a purple solid. The solid was recrystallized from CH$_3$CN/ether affording purple crystals suitable for X-ray diffraction. Solid **4**(ClO$_4$)$_2$ slowly decomposes at room temperature even under inert atmosphere and should be kept in a freezer. Anal. Calcd for **4**(ClO$_4$)$_2$ or C$_{58}$H$_{54}$Cl$_2$Fe$_2$N$_8$O$_{10}$ (Found): C, 57.78 (57.61); H, 4.51 (4.55); Cl, 5.88 (5.86); N, 9.29 (9.45). UV−vis (CH$_3$CN): λ_{max}, nm (ε, M^{-1} cm^{-1}), 518 (2400).

[Fe(BnBQA)(CH$_3$CN)(H$_2$O)](ClO$_4$)$_2$, 5(ClO$_4$)$_2$. BnBQA (0.39 g, 1 mmol) dissolved in CH$_2$Cl$_2$ (2 mL) was added to a vigorously stirred suspension of Fe(ClO$_4$)$_2$·6H$_2$O (0.36 g, 1.0 mmol) in CH$_2$Cl$_2$ (3 mL). The mixture was stirred overnight and dried in vacuo to afford a yellow powder. Recrystallization by layering ether onto a CH$_3$CN solution affords the product as large pale yellow plates (0.67 g, 93%). Anal. Calcd for C$_{29}$H$_{28}$Cl$_2$FeN$_4$O$_9$ (Found): C, 49.52 (49.82); H, 4.01 (3.94); N, 7.97 (8.35); Cl, 10.08 (10.39).

[Fe$_3$(μ-O)$_3$(TPA)$_3$](OTf)$_3$, 6(OTf)$_3$. Dark gray-green crystals of this trinuclear complex were obtained by exposure of **1**(OTf)$_2$ in CH$_3$CN to O$_2$ and slow diffusion of diethyl ether into this solution. Yield: 95%. ES-MS: m/z 1384 (M − CF$_3$SO$_3$)$^+$. Anal. Calcd for **6**(OTf)$_3$ or C$_{57}$H$_{54}$F$_9$Fe$_3$N$_{12}$O$_{12}$S$_3$ (Found): C, 44.63 (43.83); H, 3.55 (3.46); N, 10.96 (11.17). UV−vis (CH$_3$CN): λ_{max}, nm (ε, M^{-1} cm^{-1}): 490 (320), 530 (350), 595 (250).

Generation of Dioxygen Adducts. A solution of a diiron(II) complex (**1**, **3**, or **4**) was put into a gastight cuvette, cooled to low temperature, and slowly purged with dioxygen. The progress of the reactions can be monitored by the development of a deep-green color. The optimal conditions found for the generation of the O$_2$ adducts were the following: CH$_2$Cl$_2$ solution and $T = -80$ °C for **1·O$_2$**; CH$_2$Cl$_2$ solution with 2 equiv of Et$_3$N (vs **3**) and $T = -80$ °C for **3·O$_2$**; MeCN solution and $T = -40$ °C for **4·O$_2$**. UV−vis, λ_{max}, nm (ε, M^{-1} cm^{-1}), **1·O$_2$** 490 (1100), 640 (1100); **3·O$_2$** 480 (1000), 620 (1000); **4·O$_2$** 502 (1300), 650 (1300). The relative yields of the O$_2$ adducts under other conditions were estimated on the basis of these extinction coefficients.

Titration of Diiron(II) Complexes with O$_2$. A solution of a diiron(II) complex (**1−4,** typically 0.3 mM) was put into a gastight optical cuvette with a septum and titrated at room temperature with air-saturated solvent (1.2 mM O$_2$ in CH$_2$Cl$_2$ or 1.7 mM O$_2$ in MeCN)[33−35] using a graduated syringe. The progress of titration was monitored by visible spectrophotometry.

Physical Methods. Room temperature UV−vis spectra were acquired on a Hitachi 2000 spectrophotometer. Low temperature visible spectra were recorded on a Hewlett-Packard 8452 diode array spectrophotometer using an immersion Dewar equipped with quartz windows and filled with methanol chilled with liquid N$_2$. ^{1}H NMR spectra were recorded on a Varian Unity 300 or 500 spectrometer

(32) Wei, N.; Murphy, N. N.; Narasimba, N.; Chen, Q.; Zubieta, J.; Karlin, K. D. *Inorg. Chem.* **1994**, *33*, 1953−1965.

(33) Battino, R. *Oxygen and Ozone*; Battino, R., Ed.; Pergamon Press: New York, 1981; Vol. 8.

(34) Achord, J. M.; Hussey, C. L. *Anal. Chem.* **1980**, *52*, 601−602.

(35) Sawyer, D. T.; Chiericato, G.; Angelis, C. T.; Nanni, E. J.; Tsuchiya, T. *Anal. Chem.* **1982**, *54*, 1720−1724.

Table 1. Crystallographic Data

	1(OTf)$_2$·CH$_3$CN (6-Me$_3$-TPA)	**2**(ClO$_4$)$_2$·2CH$_3$OH (TPA)	**2**(OTf)$_2$ (TPA)	**3**(OTf)$_2$·2CH$_3$CN (BQPA)	**4**(ClO$_4$)$_2$ (BnBQA)
formula	C$_{46}$H$_{53}$F$_6$Fe$_2$N$_9$O$_8$S$_2$	C$_{38}$H$_{46}$Cl$_2$Fe$_2$N$_8$O$_{12}$	C$_{38}$H$_{38}$F$_6$Fe$_2$N$_8$O$_8$S$_2$	C$_{58}$H$_{52}$F$_6$Fe$_2$N$_{10}$O$_8$S$_2$	C$_{58}$H$_{54}$Cl$_2$Fe$_2$N$_8$O$_{10}$
fw, amu	1149.79	989.43	1024.58	1306.92	1205.69
cryst habit, color	block, orange	plate, orange	prism, orange	cube, red-black	block, red
cryst syst	triclinic	monoclinic	monoclinic	monoclinic	orthorhombic
space group	$P\bar{1}$	$P2_1/n$	$P2_1/n$	$P2_1/c$	$Pbca$
a, Å	13.128(1)	9.9451(3)	11.6706(11)	11.6282(6)	13.518(8)
b, Å	13.816(2)	13.7240(3)	12.1665(11)	18.890(1)	18.87(1)
c, Å	15.971(2)	16.5473(3)	15.8301(14)	13.3536(8)	21.64(1)
α, deg	72.905(2)	90	90	90	90
β, deg	68.213(2)	104.012(1)	108.096(2)	98.956(1)	90
γ, deg	76.613(2)	90	90	90	90
V, Å^3	2546.4(5)	2191.3(1)	2136.5(3)	2897.4(3)	5519(6)
Z	2	2	2	2	4
D(calc), Mg m^{-3}	1.500	1.500	1.593	1.498	1.451
T, K	173(2)	173(2)	173(2)	173(2)	173(2)
μ, mm^{-1}	0.734	0.853	0.864	0.656	1.451
$R_1{}^a$	0.0489	0.0356	0.0516	0.0413	0.0587
$wR_2{}^b$	0.1264	0.0737	0.1361	0.1029	0.1066

^{a} $R = (\sum|(F_o - F_c)|)/(\sum|F_o|)$. ^{b} $R_w = (\sum[w(F_o{}^2 - F_c{}^2)^2]/(\sum[w(F_o{}^4)])^{1/2}$, where $w = q/\sigma^2(F_o{}^2) + (aP)^2 + bP$.

at ambient temperature. Chemical shifts (in ppm) were referenced to the residual protic solvent peaks.

Crystallographic Studies. Crystals of the complexes **1**(OTf)$_2$·CH$_3$CN, **2**(ClO$_4$)$_2$·2CH$_3$OH, **2**(OTf)$_2$, **3**(OTf)$_2$·2CH$_3$CN, **4**(ClO$_4$)$_2$, and **6**(OTf)$_3$·2CH$_3$CN were mounted onto glass fibers, and data were collected at −100 °C on a Siemens SMART system equipped with graphite-monochromated Mo Kα ($\lambda = 0.71073$ Å) radiation and a CCD detector (or Bruker P4 SMART CCD system for **2**(OTf)$_2$). An initial set of cell constants was calculated from reflections harvested from three sets of 20−30 frames. These initial sets of frames were oriented such that orthogonal wedges of reciprocal space were surveyed. Final cell constants for all six compounds were calculated from sets of 3560, 6719, 9587, 2999, 3525, and 3570 strong reflections from the actual data collections for **1**(OTf)$_2$·CH$_3$CN, **2**(ClO$_4$)$_2$·2CH$_3$OH, **2**(OTf)$_2$, **3**(OTf)$_2$·2CH$_3$CN, **4**(ClO$_4$)$_2$, and **6**(OTf)$_3$·2CH$_3$CN, respectively. All calculations were performed using an SGI INDY R4400-SC or Pentium computer with the SHELXTL V5.0 program suite.[36,37] Pertinent crystallographic data and experimental conditions are summarized in Table 1. All six structures were solved by direct methods. All non-hydrogen atoms were refined anisotropically, and hydrogen atoms were placed in ideal positions and refined as riding atoms with individual (or group if appropriate) isotropic displacement parameters. For **2**(ClO$_4$)$_2$·2CH$_3$OH both the hydroxide proton and the solvate methanol O−H proton were located from difference maps and were refined isotropically. Because the perchlorate anion was disordered over two positions, bond length constraints (SADI) were applied to the Cl−O bonds. Hydrogen atoms bonded to the bridging oxygen atoms were also located on the difference Fourier map for **2**(OTf)$_2$ and refined isotropically.

Electrochemistry. Cyclic voltammetry measurements were carried out in a Vacuum Atmosphere glovebox with an argon atmosphere using an EG&G PAR 273 potentiostat and a three-electrode cell (pyrolytic carbon working electrode, platinum wire auxiliary electrode, and silver pseudoreference electrode). Dry acetonitrile or dichloromethane with 0.1 M n-Bu$_4$NPF$_6$ supporting electrolyte was used as solvent for complexes **1**−**4** (ca. 2 mM). In additional experiments, a small amount of triethylamine (ca. 4 mM)

was introduced into the solvent. Ferrocene was used as an internal standard.[38] In most experiments, the range of potentials from ca. −1.6 to +0.4 V versus Fc$^+$/Fc was scanned with a rate of 100 mV min^{-1}.

ESI Mass Spectrometry. Products of oxygenation of complexes **1**−**4** at room temperature were identified by electrospray mass spectrometry using a Finnigan LTQ or a Finnigan-MAT (San Jose, CA) LCQ ion trap mass spectrometer. Acetonitrile solutions of **1**−**4** (0.1 mM) were exposed to air and subjected to analysis immediately upon a change of color to pale-yellow, characteristic of oxo-bridged oligomeric iron(III) complexes. Assignment of the major peaks in the mass spectra was confirmed by the comparison of observed values of m/z and isotopic satellite patterns with those calculated by the IsoPro 3.0 software.

Kinetic Measurements. The kinetics of the oxygenation of complexes **1**−**4** was studied using a Hi-Tech Scientific (Salisbury, Wiltshire, U.K.) SF-43 multimixing anaerobic cryogenic stopped-flow instrument combined with either a monochromator (low intensity light irradiation of the sample) or a diode array rapid scanning unit (strong UV−vis irradiation of the sample). No difference in spectral and kinetic data was observed for the monochromator and diode array modes in this study, indicating the absence of photosensitivity. All manipulations with complexes **1**−**4** and their solutions were done using an argon atmosphere glovebox, airtight syringes, and the anaerobic stopped-flow instrument to avoid contamination with air. Saturated solutions of O$_2$ in CH$_2$Cl$_2$ and CH$_3$CN were prepared by bubbling the dry O$_2$ gas for 20 min in a septum-closed cylinder with the solvent at a constant temperature (20 or 25 °C). The solubility of O$_2$ was accepted to be 5.8 mM in dichloromethane at 20 °C and 8.1 mM in acetonitrile at 25 °C.[33−35] Solutions with lower O$_2$ concentrations were prepared from graduated mixtures of oxygen and nitrogen gases assuming the linear dependency of solubility on the partial pressure of gas. The solutions of a diiron(II) complex and O$_2$ were cooled to a preset temperature in the stopped-flow instrument before mixing. The concentrations of the reactants were corrected for the 1:1 mixing ratio and the temperature contraction of solvent (Tables S1 and S2). The densities of CH$_3$CN and CH$_2$Cl$_2$ at different temperatures were determined experimentally as described elsewhere.[27] The density of CH$_3$CN at temperatures from −40 to +25 °C could be

(36) *SHELXTL 5.10 (PC/NT-Version). Program library for Structure Solution and Molecular Graphics*; Bruker Analytical X-ray Systems: Madison, WI, 1998.

(37) Sheldrick, G. M. *SHELXL-97. Program for the Refinement of Crystal Structure*; University of Gottingen: Gottingen, Germany, 1997.

(38) Gagné, R. R.; Koval, C. A.; Lisensky, G. C. *Inorg. Chem.* **1980**, *19*, 2854−2855.

satisfactorily described by a linear equation: d_T (g/cm^3) = 0.805(5) − 0.00108(2) × T (T in °C). The density of CH$_2$Cl$_2$ could be satisfactorily described by the following linear equation: d_T (g/cm^3) = 1.370(5) − 0.00180(2) × T (T in °C).[27]

For the kinetic experiments, dioxygen was always taken in large excess so that its concentration does not change significantly during the reaction with a diiron(II) complex. The kinetic traces obtained under the pseudo-first-order conditions over 3−5 half-lives were fit to eq 1.

$$A_t = A_\infty - (A_\infty - A_o)\cdot\exp(-k_{obs}t) \qquad (1)$$

The fit of experimental data to eq 1 and the independence of k_{obs} on [Fe$_2$] served as proof of the first-order behavior of the reactions in the diiron(II) complex. A linear dependence of k_{obs} on [O$_2$] served as proof of the first-order behavior of the reactions in dioxygen. Equation 2 was used to calculate the second-order rate constant k.

$$k = k_{obs}/[O_2] \qquad (2)$$

$$-d[Fe_2]/dt = k_{obs}[Fe_2] = k[O_2][Fe_2] \qquad (3)$$

The values of k (M^{-1} s^{-1}) were determined at different temperatures and fit to the Eyring eq 4 to obtain the activation parameters $\Delta H^{\ddagger}$ and $\Delta S^{\ddagger}$.

$$\ln(k/T) = 23.76 + \Delta S^{\ddagger}/R - \Delta H^{\ddagger}/RT \qquad (4)$$

In some cases, the formation of an oxygen adduct from the diiron(II) precursor and O$_2$ was closely followed by the decomposition of the adduct. Then the kinetic traces were fit to a two-exponential eq 5.

$$A_t = A_\infty + \Delta A_1\cdot\exp(-k_{obs}t) + \Delta A_2\cdot\exp(-k_{decomp}t) \qquad (5)$$

The values of k_{obs} (corresponding to the formation of the oxygen adduct) were treated as described above. Kinetic data are summarized in Tables S3−S18 and Figures S1−S26.

Results

Diiron(II) Precursors. Synthesis and Solution Characterization. The reaction of iron(II) triflate or perchlorate with an equimolar amount of a tetradentate aminopyridine ligand L (L = 6-Me$_3$-TPA, TPA, or BQPA) and an equimolar amount of NaOH in methanol afforded complexes [Fe^{II}$_2$(μ-OH)$_2$L$_2$]$^{2+}$ (**1**−**3**). Using a similar procedure, with the tridentate ligand BnBQA in acetonitrile and Et$_3$N as base, gave the complex [Fe$_2$(μ-OH)$_2$(BnBQA)$_2$(CH$_3$CN)$_2$]$^{2+}$ (**4**). These four diiron(II) complexes were characterized by X-ray crystallography as triflate or perchlorate salts (vide infra). Complex **4**(ClO$_4$)$_2$ had limited stability in the solid state even under anaerobic conditions. It was then found that the corresponding mononuclear complex [Fe(BnBQA)(CH$_3$CN)(H$_2$O)](ClO$_4$)$_2$, **5**(ClO$_4$)$_2$, obtained from a combination of Fe(ClO$_4$)$_2$·6H$_2$O and BnBQA in CH$_2$Cl$_2$/CH$_3$CN by omitting the addition of base, was a convenient and stable precursor to **4**, which could then easily be prepared in situ in nearly quantitative yields (as determined by UV−vis spectrophotometry) by treatment of a CH$_3$CN solution of **5** with 1 equiv of triethylamine.

Figure 1 shows the visible spectra of complexes **1**−**4**, which are dominated by iron(II)-to-pyridine (or quinoline)
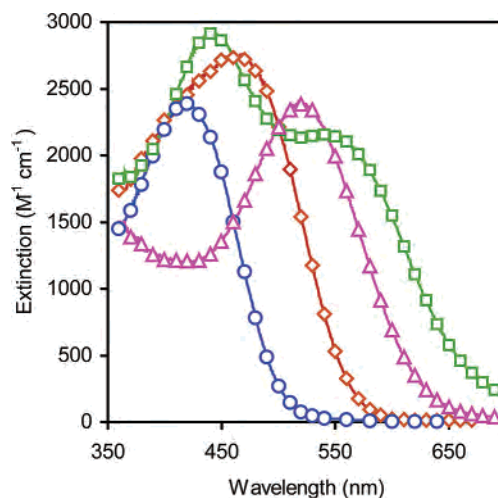

Figure 1. UV−vis spectra of the diiron(II) complexes **1** (○), **2** (◇), **3** (□), and **4** (△) in acetonitrile solution.

charge-transfer transitions. The absorbance maximum of **1** at 420 nm is observed to red-shift to 465 nm in **2**, consistent with the expected decrease in the Lewis acidity of the metal center upon replacement of 6-Me$_3$-TPA with TPA.[39] The absorbance maxima of **3** and **4** are even more red-shifted due to the presence of the quinoline ligands that have lower energy π-acceptor orbitals for the MLCT transitions. Interestingly, **3**, a complex with mixed pyridine and quinoline ligation, exhibits a spectrum with two absorbance features at 440 and 560 nm; these features may be assigned, respectively, to the iron(II)-to-pyridine and the iron(II)-to-quinoline charge-transfer transitions.

Structural Characterization of the Complexes with Fe^{II}$_2$(OH)$_2$ Diamond Cores. Single crystals of **1**(OTf)$_2$·CH$_3$CN, **2**(OTf)$_2$, **2**(ClO$_4$)$_2$·2CH$_3$OH, **3**(OTf)$_2$·2CH$_3$CN, and **4**(ClO$_4$)$_2$ suitable for X-ray diffraction studies were grown from CH$_3$CN/Et$_2$O or CH$_3$OH/Et$_2$O. Figure 2 shows the structures of the complex cations in **1**−**4**, and Table 2 lists selected bond lengths and angles. The structure of complex **1** as the perchlorate salt **1**(ClO$_4$)$_2$ has been published[26] and is very similar to that found for the triflate salt **1**(OTf)$_2$·CH$_3$CN reported here. Likewise, the geometric parameters of complex **2** are very close in the crystals of **2**(OTf)$_2$ and **2**(ClO$_4$)$_2$·2CH$_3$OH. Examination of the structures reveals that **1**−**4** all contain a centrosymmetric Fe^{II}$_2$(μ-OH)$_2$ diamond core (Scheme 3). Four nitrogen atoms of the tetradentate ligand in **1**−**3** or the tridentate ligand plus CH$_3$CN in **4** complete the distorted octahedral coordination environment about each iron center. The Fe^{II}$_2$(μ-OH)$_2$ diamond cores have C_{2h} symmetry with asymmetric Fe−O(H)···Fe units; a similar asymmetry is observed in related diiron(II) complexes reported by Lippard and co-workers having a single hydroxo or methoxo bridge, [Fe$_2$(BPMAN)(μ-OH or OMe)(μ-O$_2$CR)]-(OTf)$_2$.[40,41] The asymmetry appears to be determined by the nature of the *trans* ligand; the shorter Fe^{II}−μ-OH bond

(39) Zang, Y.; Kim, J.; Dong, Y.; Wilkinson, E. C.; Appelman, E. H.; Que, L., Jr. *J. Am. Chem. Soc.* **1997**, *119*, 4197−4205.

(40) He, C.; Lippard, S. J. *Inorg. Chem.* **2001**, *40*, 1414−1420.

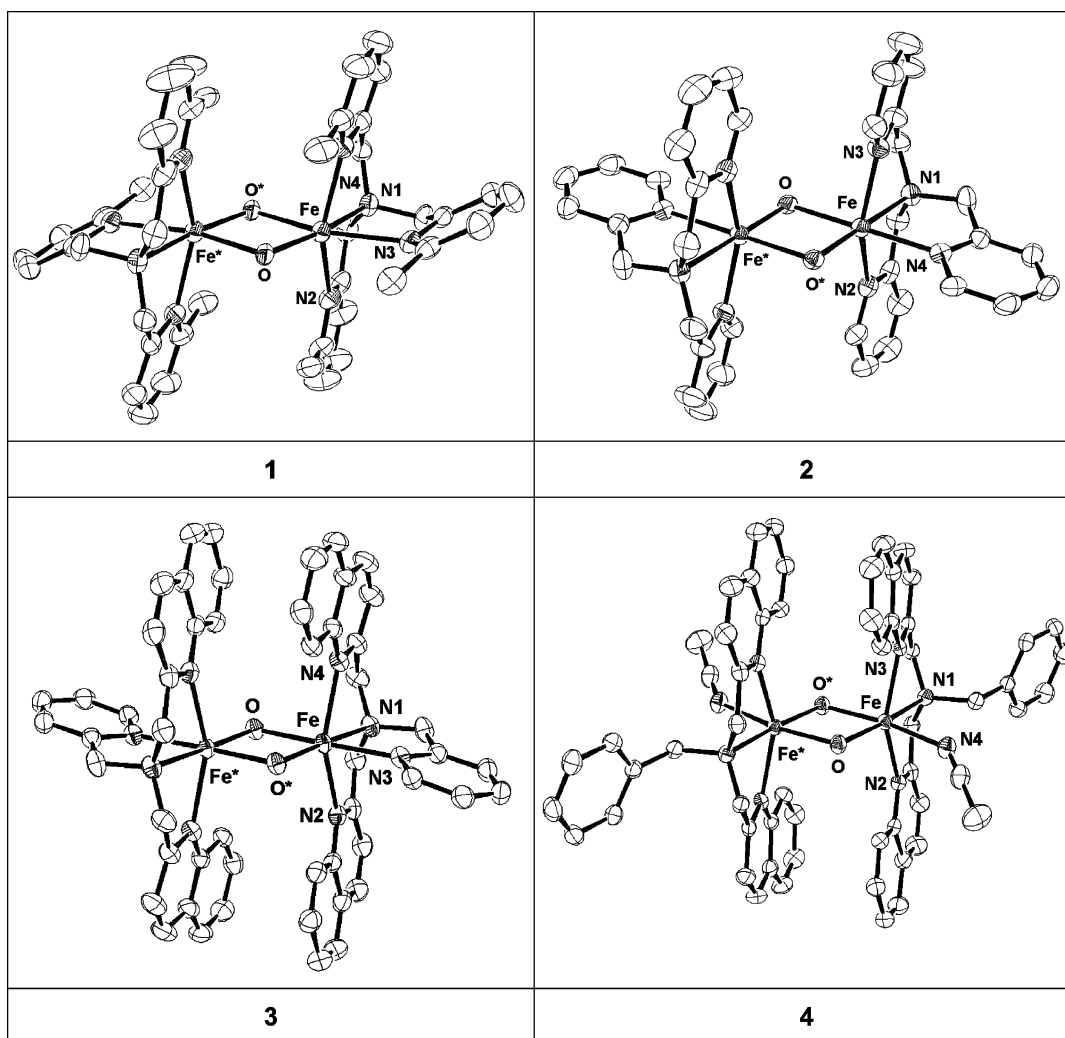(41) Kuzelka, J.; Mukhopadhyay, S.; Spingler, B.; Lippard, S. J. *Inorg. Chem.* **2003**, *42*, 6447−6457.

Figure 2. ORTEP representations of the X-ray crystal structures of the bis(μ-hydroxo)diiron(II) complex cations **1−4** showing 50% probability thermal ellipsoids. Hydrogen atoms are omitted for clarity.
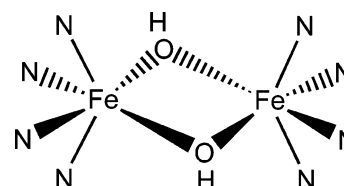
Table 2. Selected Bond Lengths (Å) and Bond Angles (deg) for Bis(μ-hydroxo)diiron(II) Complexes **1−4**[a]

	1(ClO$_4$)$_2$[b]	**1**(OTf)$_2$·CH$_3$CN[c]	**2**(ClO$_4$)$_2$·2CH$_3$OH	**2**(OTf)$_2$	**3**(OTf)$_2$·2CH$_3$CN	**4**(ClO$_4$)$_2$
ligand	6-Me$_3$-TPA	6-Me$_3$-TPA	TPA	TPA	BQPA	BnBQA
Fe−O	1.973(2) (O1)	1.995(2)/2.032(2) (O1)	2.0059(15) (O1*)	1.9726(17) (O1)	1.9837(14) (O1)	1.985(2) (O1)
	2.168(2) (O1*)	2.182(2)/2.208(2) (O1*)	2.1595(16) (O1)	2.1344(18) (O1*)	2.1007(15) (O1*)	2.090(2) (O1*)
Fe−N$_{am}$ (in-plane)	2.222(2) (N1)	2.230(3)/2.213(3) (N1)	2.253(2) (N1)	2.264(2) (N1)	2.2421(18) (N1)	2.254(3) (N1)
Fe−N$_{py}$ (in-plane)	2.285(2) (N3)	2.333(3)/2.307(3) (N3)	2.191(2) (N4)	2.189(2) (N3)	2.1698(18) (N3)	
Fe−N$_{MeCN}$ (in-plane)						2.290(3) (N4)
Fe−N$_{py}$ (out-of-plane)	2.326(3) (N2)	2.306(3)/2.336(3) (N2)	2.226(2) (N2)	2.205(2) (N2)	2.3057(19) (N2)	2.252(3) (N2)
	2.290(3) (N4)	2.282(3)/2.287(3) (N4)	2.235(2) (N3)	2.192(2) (N4)	2.2880(19) (N4)	2.254(3) (N3)
Fe⋯Fe*	3.187	3.175/3.221	3.087	3.010	3.086	3.135
Fe−O−Fe*	100.55(9)	98.82(10)/98.75(10)	95.57(6)	94.20(7)	98.11(6)	100.54(11)
O−Fe−O *	79.45(9)	81.18(10)/81.25(10)	84.43(6)	85.80(7)	81.89(6)	79.46(11)

[a] Diiron core is depicted in Scheme 2; ORTEP views of complex cations are shown in Figure 2. [b] Data from ref 26. [c] There are two crystallographically independent dimers in the formula unit, both with inversion centers at their molecular centers.

(1.97−2.01 Å in **1−4**) is associated with the hydroxide *trans* to the tertiary amine, while the longer Fe^{II}−(μ-OH) bond (2.09−2.21 Å in **1−4**) is associated with the hydroxide *trans* to the pyridine or CH$_3$CN ligand. Indeed, in the Fe$^{II}_2$(μ-OH)$_2$ complexes with capping ligands having identical donor atoms the Fe^{II}−(μ-OH) bonds are almost equivalent as in [Fe$_2$(μ-OH)$_2$(κ^2-PhTp^{tBu})$_2$] (1.974 and 1.978 Å),[42] [Fe$_2$(μ-OH)$_2$(κ^3-

(42) Kisko, J. L.; Hascall, T.; Parkin, G. *J. Am. Chem. Soc.* **1998**, *120*, 10561−10562.

Scheme 3. Coordination Environment of the Iron(II) Centers in Complexes **1−4**

PhTp^{iPr_2})$_2$] (2.016 and 2.04 Å),[43] and [Fe$_2$(μ-OH)$_2$(κ^4-BPMCN)$_2$] (2.05 and 2.08 Å).[44] The shorter Fe^{II}−(μ-OH)
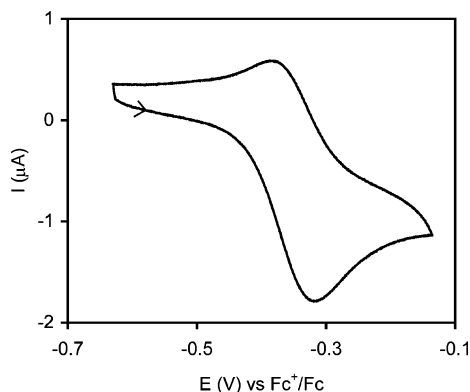
Figure 3. Cyclic voltammogram of 2 mM [Fe^{II}$_2$(μ-OH)$_2$(BQPA)$_2$](OTf)$_2$ (**3**) in MeCN with 0.1 M [n-Bu$_4$N][PF$_6$] as a supporting electrolyte (scan rate 100 mV s^{-1}).

Table 3. Fe^{III}Fe^{II}/Fe^{II}Fe^{II} Redox Potentials (mV vs Fc$^+$/Fc^0) for Bis(μ-hydroxo)diiron Complexes

diiron(II) species	$E_{1/2}$ (ΔE)	reversibility	ref
1, [Fe$_2$(OH)$_2$(6-Me$_3$-TPA)$_2$]$^{2+}$ (in CH$_2$Cl$_2$)	−150 (95)	QR	this work
1, [Fe$_2$(OH)$_2$(6-Me$_3$-TPA)$_2$]$^{2+}$ (in CH$_2$Cl$_2$/Et$_3$N)	−100^a	IRR	this work
1, [Fe$_2$(OH)$_2$(6-Me$_3$-TPA)$_2$]$^{2+}$ (in MeCN)	−160 (100)	QR	this work
1, [Fe$_2$(OH)$_2$(6-Me$_3$-TPA)$_2$]$^{2+}$ (in MeCN/Et$_3$N)	−120^a	IRR	this work
2, [Fe$_2$(OH)$_2$(TPA)$_2$]$^{2+}$ (in CH$_2$Cl$_2$)	−460 (65)	QR	this work
2, [Fe$_2$(OH)$_2$(TPA)$_2$]$^{2+}$ (in CH$_2$Cl$_2$/Et$_3$N)	−430^a	IRR	this work
2, [Fe$_2$(OH)$_2$(TPA)$_2$]$^{2+}$ (in MeCN)	−450^a	IRR	this work
2, [Fe$_2$(OH)$_2$(TPA)$_2$]$^{2+}$ (in MeCN/Et$_3$N)	−450^a	IRR	this work
3, [Fe$_2$(OH)$_2$(BQPA)$_2$]$^{2+}$ (in CH$_2$Cl$_2$)	−370 (70)	QR	this work
3, [Fe$_2$(OH)$_2$(BQPA)$_2$]$^{2+}$ (in CH$_2$Cl$_2$/Et$_3$N)	−330^a	IRR	this work
3, [Fe$_2$(OH)$_2$(BQPA)$_2$]$^{2+}$ (in MeCN)	−340 (65)	QR	this work
3, [Fe$_2$(OH)$_2$(BQPA)$_2$]$^{2+}$ (in MeCN/Et$_3$N)	−310^a	IRR	this work
4, [Fe$_2$(OH)$_2$(BnBQA)$_2$(MeCN)$_2$]$^{2+}$ (in MeCN)	−310 (95)	QR	this work
4, [Fe$_2$(OH)$_2$(BnBQA)$_2$(MeCN)$_2$]$^{2+}$ (in MeCN/Et$_3$N)	−280^a	IRR	this work
[Fe$_2$(OH)$_2$(BPMCN)$_2$]$^{2+}$ (in CH$_2$Cl$_2$)	−360	R	44
O$_2$/O$_2^-$ (in MeCN)^b	−1250	R	35, 56, 57
O$_2$/O$_2^-$ (in CH$_2$Cl$_2$)^b	−1265	R	58, 59

^{a} Anodic wave only. ^{b} The O$_2$/O$_2^-$ potential is given for comparison.

bonds in complexes **1**−**4** (1.97−2.01 Å) are comparable to those in other known (μ-hydroxo)diiron(II) complexes (1.95−2.08 Å),[40,42−45] but much longer than that for an iron(II) complex with a terminal hydroxide, [Fe(OH)(κ^3-PhTp^{tBuiPr})] (1.83 Å).[46] The longer Fe^{II}−(μ-OH) bonds in **1**−**4** (2.09−2.21 Å) are in fact among the longest of such bonds.

As noted previously, the coordination environments of the iron(II) centers are completed by the tetradentate tripodal ligand in **1**−**3** and by the meridional tridentate ligand and CH$_3$CN in **4**. In **3** and **4**, the quinoline ligands occupy the axial positions perpendicular to the FeN$_2$O$_2$ plane. The Fe−N$_{py}$ bond lengths observed (2.17−2.34 Å) are consistent with the complexes having high-spin iron(II) ions.[39] The variations in length reflect the presence or absence of an α substituent, which introduces a steric impediment that leads to the lengthening of the Fe−N$_{py}$ bond by an average of 0.09 Å.[39] The dimensions of the Fe^{II}$_2$(μ-OH)$_2$ diamond core vary little among the four complexes, as indicated by the small range of Fe−Fe distances (3.010−3.187 Å) and the Fe−O−Fe angles (94.20−100.55°). All the hydroxo bridges in **1**−**4** are hydrogen bonded to oxygen atoms of corresponding anions with O···O distances in the range of 2.77−3.15 Å.

Electrochemistry. Cyclic voltammetry (CV) experiments on complexes **1**−**4** were performed in dichloromethane and acetonitrile solutions (with 0.1 M n-Bu$_4$NPF$_6$) under inert atmosphere (Ar), except for **4**, which decomposes in CH$_2$Cl$_2$. In additional CV experiments, a small amount of triethylamine (2 equiv with respect to **1**−**4**) was introduced into the freshly prepared solutions. The range of potentials from −1.6 to +0.4 V (vs Fc$^+$/Fc) was scanned to look for the Fe^{II}Fe^{III}/Fe^{II}Fe^{II} redox couple, because for all previously reported diiron complexes with N/O-donor atoms such a couple had been found within the range (Tables 3 and S19).[40,41,44,45,47−59]

Cyclic voltammetry experiments show that the diiron(II) complexes **1**−**4** are electrochemically active and can be oxidized at potentials of −460 to −150 mV versus Fc$^+$/Fc (Figure 3, Table 3). The $E_{1/2}$ values for **1**−**4** are similar to the Fe^{II}Fe^{III}/Fe^{II}Fe^{II} potential reported for the closely related diiron complex [Fe^{II}$_2$(μ-OH)$_2$(BPMCN)$_2$]$^{2+}$ (−360 mV vs Fc$^+$/Fc), whose one-electron oxidation product [Fe^{II}Fe^{III}(μ-OH)$_2$(BPMCN)$_2$]$^{3+}$ has been isolated and structurally characterized.[44] The electrochemical oxidations are quasireversible in CH$_2$Cl$_2$ and MeCN and essentially solvent-independent, except for **2**, where the simple change of solvent from CH$_2$Cl$_2$ to MeCN caused the loss of reversibility. Apparently, the oxidized Fe^{II}Fe^{III} form of **2** is unstable in MeCN. A byproduct, the mononuclear complex [Fe(TPA)(MeCN)$_2$]$^{2+}$, showed its prominent redox feature (a reversible wave at +750 mV vs Fc$^+$/Fc) after repeated electrochemical cycling of **2** in MeCN. A similar instability in MeCN has been observed for the mixed valence complex [Fe^{II}Fe^{III}(OH)$_2$-(BPMCN)$_2$]$^{3+}$, which could be isolated and crystallized only from CH$_2$Cl$_2$.[44] In these cases, the formation of highly stable low-spin mononuclear iron(II) complexes may serve as a thermodynamic sink that destroys the mixed-valent Fe^{II}Fe^{III} species and leads to irreversibility of the diiron redox couples.[45,60,61] It should be noted that the TPA complex is

(43) Kitajima, N.; Tamura, N.; Tanaka, M.; Moro-oka, Y. *Inorg. Chem.* **1992**, *31*, 3342−3343.
(44) Stubna, A.; Jo, D.-H.; Costas, M.; Brenessel, W. W.; Andres, H.; Bominaar, E. L.; Münck, E.; Que, L., Jr. *Inorg. Chem.* **2004**, *43*, 3067−3079.
(45) Hartman, J. R.; Rardin, R. L.; Chaudhuri, P.; Pohl, K.; Wieghardt, K.; Nuber, B.; Weiss, J.; Papaefthymiou, G. C.; Frankel, R. B.; Lippard, S. J. *J. Am. Chem. Soc.* **1987**, *109*, 7387−7396.
(46) Hikichi, S.; Ogihara, T.; Fujisawa, K.; Kitajima, N.; Akita, M.; Moro-oka, Y. *Inorg. Chem.* **1997**, *36*, 4539−4547.

(47) Stassinopoulos, A.; Schulte, G.; Papaefthymiou, G. C.; Caradonna, J. P. *J. Am. Chem. Soc.* **1991**, *113*, 8686−8697.
(48) Mukerjee, S.; Stassinopoulos, A.; Caradonna, J. P. *J. Am. Chem. Soc.* **1997**, *119*, 8097−8098.
(49) Suzuki, M.; Uehara, A.; Oshio, H.; Endo, K.; Yanaga, M.; Kida, S.; Saito, K. *Bull. Chem. Soc. Jpn.* **1987**, *60*, 3547−3555.

unique in its properties in the series of related mononuclear iron(II) species, $[Fe(L)(MeCN)_n]^{2+}$ (L = TPA, BQPA, 6-Me$_3$-TPA, BnBQA). Only the TPA complex is low-spin[39,62,63] and may therefore possess exceptional stability.

The half-wave potentials for the one-electron oxidation of complexes **1**−**4** fall in the middle of the range reported in the literature for the Fe^{II}Fe^{III}/Fe^{II}Fe^{II} redox pairs (Tables 3 and S19), which vary significantly depending on the charge, donor properties, and topology of the ligands. The lowest potentials (about −1000 mV vs Fc$^+$/Fc) were found for complexes $[Fe_2(H_2Hbab)_2(DMF)_2(N\text{-}MeIm)]^0$ and $[Fe_2(H_2bamb)_2\text{-}(N\text{-}MeIm)_2]^0$ with two negatively charged and strongly donating phenolate groups on each tetradentate ligand.[47,48] At the other limit, a relatively high potential of about +300 mV versus Fc$^+$/Fc was observed for complex $[Fe_2(BPMAN)\text{-}(O_2CR)_2]^{2+}$ with a neutral polydentate aminopyridine ligand BPMAN and weakly donating bridging carboxylates.[40,41]

Hydroxide bridges modulate the redox properties of dinuclear iron complexes. For example, the substitution of a carboxylate ligand in $[Fe_2(BPMAN)(O_2CPhCy)_2]^{2+}$ with a better-donating hydroxide caused the shift of the Fe^{II}Fe^{III}/Fe^{II}Fe^{II} potential from +296 mV versus Fc$^+$/Fc in $[Fe_2\text{-}(BPMAN)(O_2CPhCy)_2]^{2+}$ to −22 mV versus Fc$^+$/Fc in $[Fe_2(BPMAN)(O_2CPhCy)(OH)]^{2+}$.[40] As expected, even more negative potentials (ranging from −150 to −460 mV) were found in our work for complexes **1**−**4** that contain tetradentate aminopyridine ligands similar to BPMAN but have two hydroxo-bridges between two iron(II) centers. The effect is especially dramatic if one compares an Fe^{III}L/Fe^{II}L potential for a monomeric complex $[Fe(TPA)(MeCN)_2]^{2+}$ (+750 mV) to an Fe^{III}Fe^{II}/Fe^{II}Fe^{II} potential for the corresponding bis-hydroxo bridged complex **2** (−450 mV).

Although reversible oxidation and stable mixed-valent(II,III) species were observed for several diiron(II,II) complexes of dinucleating ligands with bridging carboxylates,[40,49−53] introduction of the bridging OH-ligands into the diiron(II,II) complexes usually led to quasireversible electrochemical oxidation.[45,49,50] A possible reason for the

quasireversibility is the deprotonation of the OH-ligand upon oxidation to the Fe^{II}Fe^{III} state.[45] In our experiments, addition of a small amount of Et$_3$N to the solvent (either CH$_2$Cl$_2$ or CH$_3$CN) did not shift the anodic peak of complexes **1**−**4**, but it caused the cathodic counter peaks to disappear. Apparently, triethylamine does not remove protons from the Fe^{II}Fe^{II} complexes but may deprotonate the Fe^{II}Fe^{III} species leading to the disintegration of the oxidized complexes. As a result, the Fe^{II}Fe^{III}/Fe^{II}Fe^{II} couples lose their reversibility. Extending the anodic range of potentials in CH$_2$Cl$_2$ solutions of **1**−**3** revealed an additional irreversible wave at +520 mV versus Fc$^+$/Fc, attributed to the oxidation of Et$_3$N.

The Fe^{II}Fe^{III}/Fe^{II}Fe^{II} redox potentials increase in the series **2** < **3** ∼ **4** < **1**, which may be explained by the weakening donor properties of the N-ligands with the introduction of substituents at the pyridine 6-position. Indeed, BQPA is derived from TPA by adding two electron-withdrawing benzo groups. Ligand BnBQA contains the same two additional benzo groups and lacks one pyridine donor, which is substituted for a weaker donor, MeCN, in complex **4**. Finally, ligand 6-Me$_3$-TPA contains three 6-methyl substituents that interfere sterically with the coordination of the pyridine N-atoms.[39] There is a positive correlation between the average Fe−N bond lengths in complexes **1**−**4** and their oxidation potentials (Figure S27), indicating that longer (and weaker) Fe−N bonds destabilize the higher oxidation state of the diiron complexes. The connection between long metal−ligand bonds and high redox potentials has also been noted for (hexaamine)cobalt(II/III) complexes[64] and may be true in general for complexes with predominantly σ-donor ligands.[65,66]

As mentioned above, incorporating two hydroxo bridges into diiron complexes decreases the Fe^{II}Fe^{III}/Fe^{II}Fe^{II} redox potentials and makes diiron(II) complexes **1**−**4** more susceptible to oxidation. Comparing these redox potentials (−460 to −150 mV vs Fc$^+$/Fc) to the much lower potential for a one-electron reduction of O$_2$ into superoxide (ca. −1250 mV vs Fc$^+$/Fc in MeCN or CH$_2$Cl$_2$, Table 3[35,56−59]) shows, however, that the outer-sphere one-electron oxidation of **1**−**4** with O$_2$ in these solvents is a thermodynamically uphill process. Moreover, the redox potentials for other known diiron(II,II) complexes (Table S19) show that none of them can be an effective outer-sphere reducing agent for molecular oxygen in aprotic organic solvents. Coordination of the O$_2$ molecule to an iron center with subsequent inner-sphere electron transfer events (eventually yielding a coordinated peroxide) is expected to be the likely mechanism for the oxygenation of complexes **1**−**4** and related species.

Reactions with O$_2$. Overview. Table 4 summarizes the results from the reactions of **1**−**4** with O$_2$ in different solvents; a detailed discussion for each complex follows in the subsections below. Complexes **1**, **3**, and **4** (but not **2**) formed O$_2$ adducts in nearly quantitative yield at low temperature under the appropriate conditions. The adducts exhibit two comparably intense absorbance maxima near 450

(50) Suzuki, M.; Oshio, H.; Uehara, A.; Endo, K.; Yanaga, M.; Kida, S.; Saito, K. *Bull. Chem. Soc. Jpn.* **1988**, *61*, 3907−3913.

(51) Suzuki, M.; Fujinami, S.; Hibino, T.; Hori, H.; Maeda, Y.; Uehara, A.; Suzuki, M. *Inorg. Chim. Acta* **1998**, *283*, 124−135.

(52) Mashuta, M. S.; Webb, R. J.; Oberhausen, K. J.; Richardson, J. F.; Buchanan, R. M.; Hendrickson, D. N. *J. Am. Chem. Soc.* **1989**, *111*, 2745−2746.

(53) Borovik, A. S.; Papaefthymiou, V.; Taylor, L. F.; Anderson, O. P.; Que, L., Jr. *J. Am. Chem. Soc.* **1989**, *111*, 6183−6195.

(54) Buchanan, R. M.; Mashuta, M. S.; Richardson, J. F.; Oberhausen, K. J.; Hendrickson, D. N.; Webb, R. J.; Nanny, M. A. *Inorg. Chem.* **1990**, *29* (9), 1299−1301.

(55) Lee, D.; Krebs, C.; Huynh, B. H.; Hendrich, M. P.; Lippard, S. J. *J. Am. Chem. Soc.* **2000**, *122*, 5000−5001.

(56) Ohsaka, T.; Tsushima, M.; Tokuda, K. *Bioelectrochem. Bioenerg.* **1993**, *31*, 289−300.

(57) Vasudevan, D.; Wendt, H. *J. Electroanal. Chem.* **1995**, *192*, 69−74.

(58) Peover, M. E.; White, B. S. *J. Chem. Soc., Chem. Commun.* **1965**, 183−184.

(59) Ruiz, J.; Astruc, D. *C. R. Acad. Sci., Ser. IIc: Chim.* **1998**, *1*, 21−27.

(60) Armstrong, W. H.; Spool, A.; Papaefthymiou, G. C.; Frankel, R. B.; Lippard, S. J. *J. Am. Chem. Soc.* **1984**, *106*, 3653−3667.

(61) Costas, M.; Que, L., Jr. *Angew. Chem., Int. Ed.* **2002**, *41*, 2179−2181.

(62) Diebold, A.; Hagen, K. S. *Inorg. Chem.* **1998**, *37*, 215−223.

(63) Chen, K.; Que, L., Jr. *J. Am. Chem. Soc.* **2001**, *123*, 6327−6337.

(64) Comba, P.; Sickmüller, A. F. *Inorg. Chem.* **1997**, *36*, 4500−4507.

(65) Gutmann, V. *Struct. Bonding* **1973**, *15*, 141−166.

(66) Lever, A. B. P. *Inorg. Chem.* **1990**, *29*, 1271−1285.

Table 4. Properties of the Diiron(II) Peroxo Intermediates Derived from the Oxygenation of Complexes **1**−**4** in Different Solvents

complex	solvent (temp)	yield, %[a]	UV−vis λ_{max}, nm (ϵ, M^{-1} cm^{-1})	resonance Raman ν(Fe−O), ν(O−O)/ cm^{-1}	oxidation products[b]
1 (L = 6-Me$_3$-TPA)	CH$_2$Cl$_2$ (<−50 °C)	∼100%	490 (1100), 640 (1100)	465, 844[c]	[Fe$^{III}_2$(O)$_2$(L)$_2$]$^{2+}$ and
	CH$_3$CN (−40 °C)	25%			[Fe$^{III}_2$(O)(OH)(L)$_2$]$^{3+}$
2 (L = TPA)	CH$_2$Cl$_2$ (<−50 °C)	not observed	n/a		[Fe$^{III}_3$(O)$_3$(L)$_2$]$^{3+}$
	CH$_3$CN (−40 °C)				
3 (L = BQPA)	CH$_2$Cl$_2$ (<−50 °C)	not observed	480 (1000), 620 (1000)	462, 848	[Fe$^{III}_2$(O)$_2$(L)$_2$]$^{2+}$ and
	CH$_2$Cl$_2$/NEt$_3$[d] (<−50 °C)	∼100%			[Fe$^{III}_2$(O)(OH)(L)$_2$]$^{3+}$
	CH$_3$CN (−40 °C)	35%			
	CH$_3$CN/NEt$_3$[d] (−40 °C)	70%			
4 (L = BnBQA)	CH$_3$CN (−40 °C)	∼100%	502 (1300), 650 (1300)	470, 843	[Fe$^{III}_2$O$_2$(BnBQA)$_2$]$^{2+}$ and
					[BnBQA·H]$^+$

[a] The yields were estimated on the basis of extinction coefficients obtained from visible spectral data on samples evaluated by Mössbauer spectroscopy. [b] Products obtained upon warming of the peroxo intermediates to room temperature or directly upon oxygenation of diiron(II) complexes at room temperature. [c] From ref 26. [d] 2 mol of triethylamine per mol of **3** is required; NEt$_3$ may be substituted for other noncoordinating amines.
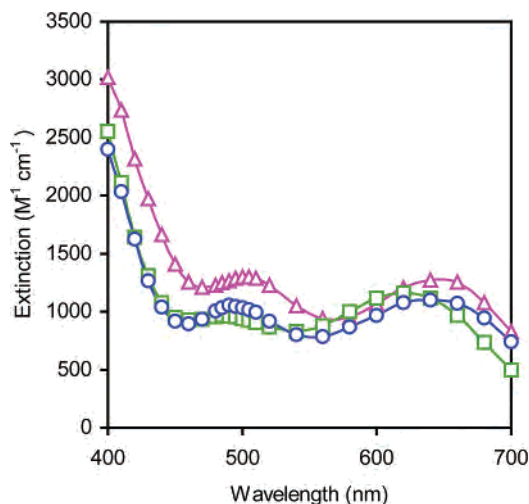

**Figure 4.** Visible spectra of the peroxo diiron(III) complexes **1·O$_2$** (○), **3·O$_2$** (□), and **4·O$_2$** (△).

and 650 nm (Figure 4) that have been previously associated with (μ-oxo)(μ-1,2-peroxo)diiron(III) complexes.[26,67,68] The presence of a μ-1,2-peroxo ligand in **3·O$_2$** and **4·O$_2$** was also confirmed by the observation of characteristic Fe−O and O−O vibrations by resonance Raman spectroscopy (Table 4), as previously detailed for **1·O$_2$**.[26] Of particular interest is the observation that **3** gave rise to a peroxo intermediate in CH$_2$Cl$_2$ only in the presence of added base (e.g., triethylamine). Formation of the peroxo complexes proceeds according to the generalized eq 6.

$$[Fe^{II}_2(\mu\text{-OH})_2L_n]^{2+} + O_2 \rightarrow [Fe_2(\mu\text{-O})(\mu\text{-O}_2)L_n]^{2+} + H_2O \tag{6}$$
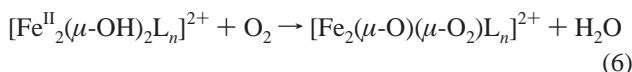
The accumulation of peroxo intermediates suggests that these species are chemically fairly stable at low temperatures and do not react with their diiron(II) precursors at an appreciable rate. Indeed, in a separate experiment we observed that preformed [Fe$_2$(μ-O)(μ-O$_2$)(6-Me$_3$TPA)$_2$]$^{2+}$ did not react with added diiron(II) precursor **1**; similar observations were made for **4**.

(67) Dong, Y.; Zang, Y.; Shu, L.; Wilkinson, E. C.; Que, L., Jr.; Kauffmann, K.; Münck, E. *J. Am. Chem. Soc.* **1997**, *119*, 12683−12684.

(68) Kodera, M.; Taniike, Y.; Itoh, M.; Tanahashi, Y.; Shimakoshi, H.; Kano, K.; Hirota, S.; Iijima, S.; Ohba, M.; Okawa, H. *Inorg. Chem.* **2001**, *40*, 4821−4822.

The peroxo intermediates, however, were thermally unstable and yielded oxo-bridged oligoiron(III) complexes upon warming. The same products were obtained if oxygenation was carried out at room temperature. The final products from the reaction of **1** or **3** and dioxygen can be identified as [Fe$^{III}_2$(μ-O)$_2$(L)$_2$]$^{2+}$ complexes, which have been previously characterized in detail.[69] The dications were readily observed by electrospray mass spectral analyses of the reaction solutions (Table 4, Figures S28−29). In the case of **3**, an additional feature was sometimes observed at m/z 463, corresponding to [Fe^{II}(BQPA)(OH)]$^+$. This feature is also present in the ES-MS spectrum of [Fe$^{III}_2$(O)(OH)(BQPA)$_2$]$^{3+}$ and is attributed to a reduction product formed under the ionization conditions during mass spectrometry. UV−vis titration experiments (Figures S5 and S12) indicate a 1:2 stoichiometry for the oxygenation reactions leading to the oxo-bridged diiron(III) complexes (eq 7).

$$2[Fe^{II}_2(\mu\text{-OH})_2L_n]^{2+} + O_2 \rightarrow 2[Fe^{III}_2(\mu\text{-O})_2L_n]^{2+} + 2H_2O \tag{7}$$
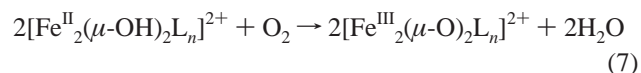
Because water is formed as a byproduct in reaction 7, protonation of the rather basic Fe$^{III}_2$(μ-O)$_2$ core can occur to afford its conjugate acid.[69] Indeed, scrutiny of the visible spectra of the product solutions from the oxidations of **1** and **3** indicates the formation of some fraction of the conjugate acid, as evidenced by significant absorbance at 550 nm that is characteristic of complexes with the Fe$^{III}_2$(μ-O)(μ-OH) core.[69]

The reaction of **4** with O$_2$ also affords [Fe$^{III}_2$O$_2$(BnBQA)$_2$]$^{2+}$, which can be observed as a prominent feature in the electrospray mass spectrum of the product solution (Figure S30). Also observed was a feature corresponding to [Fe^{II}(BnBQA)OH]$^+$. A third prominent feature can be assigned to [BnBQA·H]$^+$, suggesting the facile breakdown of the Fe$^{III}_2$(μ-O)$_2$ complex. The [Fe$^{III}_2$O$_2$(BnBQA)$_2$]$^{2+}$ complex has not been isolated and may be less stable because of the tridentate nature of the ligand, which cannot protect the Fe$^{III}_2$(μ-O)$_2$ core as well as the sterically more hindered tetradentate 6-Me$_3$-TPA and BQPA ligands.

In the reaction of **2** with O$_2$, no evidence for the corresponding dimeric [Fe$^{III}_2$(μ-O)$_2$(TPA)$_2$]$^{2+}$ complex could

(69) Zheng, H.; Zang, Y.; Dong, Y.; Young, V. G., Jr.; Que, L., Jr. *J. Am. Chem. Soc.* **1999**, *121*, 2226−2235.

Table 5. Kinetic Parameters for the Oxygenation of Diiron(II) Complexes **1**−**4** at Low Temperatures

complex (solvent/additive)	k_{obs}, s^{-1} (−40 °C, 100% O$_2$)	k, M^{-1} s^{-1} (−40 °C)	$\Delta H^{\ddagger}$, kJ mol^{-1}	$\Delta S^{\ddagger}$, J mol^{-1} K^{-1}
1 (CH$_2$Cl$_2$)	2.2(2) × 10^{-3}	0.70(7)	16(2)	−177(10)
1 (MeCN)	8.6(5) × 10^{-3}	1.94(11)	16(2)	−167(10)
2 (CH$_2$Cl$_2$)	3.8(2) × 10^{-2}	12.1(6)	30(4)	−94(10)
2 (MeCN)	3.8(3) × 10^{-2}	8.6(6)	32(4)	−87(10)
3 (CH$_2$Cl$_2$)	1.01(5) × 10^{-2}	3.2(2)	36(4)	−80(10)
3 (CH$_2$Cl$_2$/2 equiv NEt$_3$)	8(1) × 10^{-3}	2.6(3)	36(4)	−81(10)
3 (MeCN)	4.7(2) × 10^{-3}	1.07(5)	34(4)	−95(10)
3 (MeCN/2 equiv NEt$_3$)	4.5(2) × 10^{-3}	1.03(5)	33(4)	−101(10)
4 (MeCN)	11.7(5)	2670(100)	16(2)	−108(10)

be obtained although we believe that it is likely to be the initial product (reaction 7). Instead, the more stable trimer [Fe$^{III}_3$(μ-O)$_3$(TPA)$_3$]$^{3+}$ (**6**) was isolated in 95% yield and identified in solution by ES-MS (Figure S31) and its visible spectrum with maxima at 490 nm (ϵ = 320 M^{-1} cm^{-1}), 530 nm (ϵ = 350 M^{-1} cm^{-1}), and 595 nm (ϵ = 250 M^{-1} cm^{-1}), features very similar to those of previously reported [Fe$^{III}_3$(μ_2-O)$_3$(5-Et$_3$-TPA)$_3$]$^{3+}$.[69] Complex **6** was crystallographically characterized as its triflate salt (see Supporting Information, Figure S32). We postulate that the initially formed dimer product isomerizes rapidly to the more stable trimer that is observed.

Oxygenation of 1. Earlier we reported a detailed study on the oxygenation of the perchlorate salt of complex **1**, [Fe$^{II}_2$(μ-OH)$_2$(6-Me$_3$-TPA)$_2$](ClO$_4$)$_2$.[26,27] At low temperature in dichloromethane the reaction yielded quantitatively a (μ-peroxo)diiron(III) complex **1·O$_2$**, [Fe$^{III}_2$(μ-O)(μ-O$_2$)(6-Me$_3$-TPA)$_2$]$^{2+}$, which was characterized by a number of spectroscopic techniques including an EXAFS structural determination.[26,67] The triflate salt of complex **1**, [Fe$^{II}_2$(μ-OH)$_2$-(6-Me$_3$-TPA)$_2$](CF$_3$SO$_3$)$_2$, demonstrates the same chemistry. The reaction of bright-yellow **1**(OTf)$_2$ with O$_2$ in neat CH$_2$Cl$_2$ at low temperatures (−70 to −40 °C) gave in high yield the dark green dioxygen adduct **1·O$_2$** (Figures 4 and S2). The reaction of **1**(OTf)$_2$ and O$_2$ is first order in each of the reagents with a second-order rate constant k = 0.7(1) M^{-1}s^{-1} in CH$_2$Cl$_2$ at −40 °C. The dependence of k on temperature (T = −70 to −40 °C) gave the activation parameters $\Delta H^{\ddagger}$ = 16 ± 2 kJ mol^{-1} and $\Delta S^{\ddagger}$ = −177 ± 10 J mol^{-1} K^{-1} (Table S3, Figure S3). These kinetic parameters are almost identical to those obtained previously for the perchlorate salt **1**(ClO$_4$)$_2$.[27] Thus, no change in the course or kinetics of the oxygenation reaction in nonpolar solvents was found upon the substitution of the counterion from ClO$_4^-$ to CF$_3$SO$_3^-$.

In MeCN the oxygenation of **1** also gave the peroxo complex **1·O$_2$**, but its formation even at −45 °C (near the freezing point of MeCN) was closely followed by its decomposition, and the yield of **1·O$_2$** was small (25% or less). The formation of **1·O$_2$** in MeCN was first order in both **1** and O$_2$ with a second-order rate constant k = 1.9(1) M^{-1}s^{-1} at −40 °C and the activation parameters $\Delta H^{\ddagger}$ = 16 ± 2 kJ mol^{-1} and $\Delta S^{\ddagger}$ = −167 ± 10 J mol^{-1} K^{-1} (Table S4, Figure S4). The rate of oxygenation of complex **1** was somewhat higher in MeCN than in CH$_2$Cl$_2$, but the activation parameters are indistinguishable (within experimental error) for both solvents (Table 5).

Oxygenation of 2. Complex [Fe$_2$(μ-OH)$_2$(TPA)$_2$]$^{2+}$ (**2**) reacts with dioxygen in solution (CH$_3$CN or CH$_2$Cl$_2$) as seen from the color change of the solution from bright orange to pale yellow upon O$_2$ bubbling or mixing with O$_2$-containing solvent. Spectrophotometric titrations revealed that the stoichiometry of the reaction between **2** and O$_2$ is 2:1 in either CH$_3$CN or CH$_2$Cl$_2$ (Figure S5). The isolated product was the more stable [Fe$_3$(μ-O)$_3$(TPA)$_3$]$^{3+}$ (**6**) presumably derived from an initially formed [Fe$_2$(μ-O)$_2$(TPA)$_2$]$^{2+}$.

The oxidation kinetics of **2** with O$_2$ was studied in acetonitrile (T = −40 to −5 °C) and dichloromethane (T = −50 to −20 °C). No intermediates were detected during the reaction at low temperatures (Figures S5 and S6). The measurements of the pseudo-first-order rate constant at different concentrations of the reagents, [**2**]$_0$ = 0.1−0.3 mM and [O$_2$]$_0$ = 1.0−4.2 mM, showed that the reaction is first order in **2** and O$_2$ (Tables S5−S7, Figures S7−S11). The values of the second-order rate constant are quite similar in the two studied solvents, 8.6(6) M^{-1} s^{-1} in MeCN and 12.1(6) M^{-1} s^{-1} in CH$_2$Cl$_2$ at −40 °C. The activation parameters of the reaction are also nearly solvent-independent (Table 5).

Oxygenation of 3. Diiron(II) complex [Fe$_2$(μ-OH)$_2$-(BQPA)$_2$]$^{2+}$ (**3**) reacts with O$_2$ with the formation of different products depending on the nature of solvent (Table 4). In neat CH$_2$Cl$_2$, the reaction proceeds similarly to the oxygenation of **2** yielding [Fe$_2$(μ-O)$_2$(BQPA)$_2$]$^{2+}$ with no detectable intermediates even at −80 °C (Figures S12 and S13). The reaction is accompanied by a color change of the solution from dark red to brownish-yellow. However, in the presence of triethylamine (2 equiv) in CH$_2$Cl$_2$, the oxygenation of complex **3** at low temperatures (at or below −50 °C) gives nearly quantitatively a dark green dioxygen adduct **3·O$_2$** (Figure S14). At higher temperatures (−45 °C to −25 °C), the yield of **3·O$_2$** is smaller, and its decomposition becomes evident (Figures S15 and 16). The oxygenation of **3** also proceeds in neat MeCN at −40 °C, resulting in a low yield (30−35%) of **3·O$_2$** (Figure S21). A higher yield (ca. 70%) of the dioxygen adduct was obtained in MeCN in the presence of Et$_3$N (2 equiv).

Complex **3·O$_2$** can also be generated from **3** and O$_2$ in CH$_2$Cl$_2$ at low temperature in the presence of other amines (Figures S14 and S18). Diisopropylethylamine (i-Pr$_2$EtN), 1,4-diazabicyclo[2.2.2]octane (DABCO), 1,8-diazabicyclo-[4.3.0]non-5-ene (DBU), and N,N,N′,N′-tetramethylguanidine (TMG) were effective in the amount of 2 equiv (vs **3**). TMG, which is the strongest base in the series, was also effective

in a substoichiometric amount (0.5 equiv). It should be noted that the addition of the amines does not change the UV–vis spectrum of the diiron(II) precursor **3** (except for the case of DBU, where a slow decomposition process leading to the formation of a brown precipitate occurred at room temperature).

The kinetics of the reaction between **3** and O$_2$ in neat CH$_2$Cl$_2$ was studied in the temperature range from −65 to +15 °C. Dioxygen (0.60–3.2 mM) was always taken in excess relative to complex **3** (0.10–0.60 mM). Spectral changes observed by stopped-flow spectrophotometry were nearly the same as those obtained by regular spectrophotometry in the "batch" experiments, confirming that in neat CH$_2$Cl$_2$ the reaction product is the oxo-bridged diiron(III) complex [Fe$_2$(μ-O)$_2$(BQPA)$_2$]$^{2+}$ with no observable intermediates (Figures S12 and S13). The reaction between **3** and O$_2$ is first order in each of the reagents and second order overall (Figure S19, Table S12). The temperature dependence of k gave the activation parameters of the reaction as $\Delta H^{\ddagger} = 36 \pm 4$ kJ mol^{-1} and $\Delta S^{\ddagger} = -80 \pm 10$ J mol^{-1} K^{-1} (Figure S20, Table S10).

The above-mentioned experiments were carried out in rigorously dry, nonstabilized dichloromethane. No change in the reaction rate was observed when nonstabilized dichloromethane was substituted for the more usual commercial brand of dichloromethane, which contains ca. 50 mM of pentenes. Addition of small amounts of water (2–4 mM), which is in excess to the 0.5 mM concentration of complex **3**, did not change significantly the rate of oxygenation of **3** (it increased by about 20–30%), similarly to what was observed earlier for complex **1**.[27] It was impossible to increase the concentration of water in CH$_2$Cl$_2$ further without causing ice precipitation from the solution at low temperatures, which interfered strongly with the stopped-flow experiments.

The kinetics of the reaction between **3** and O$_2$ in CH$_2$Cl$_2$ solution in the presence of triethylamine (Et$_3$N, 2 equiv vs **3**) was studied by stopped-flow spectrophotometry in the temperature range from −65 to −25 °C (Figures S13 and S14). Spectral changes observed by stopped-flow spectrophotometry in the course of the reaction between **3** and O$_2$ in the presence of Et$_3$N were very similar to those obtained by regular spectrophotometry in the batch experiments and characteristic of the peroxo complex **3·O$_2$** (Figures S14 and S15). The average rate of the reaction in the presence of triethylamine decreased by ca. 20% relative to that in neat dichloromethane (Tables S10 and S11). The addition of Et$_3$N changed neither the rate law of the reaction, first order in **3** and O$_2$ (Figure S19), nor the activation parameters of the process (Figure S20).

An exploratory kinetic study was done with the other amines: i-Pr$_2$NEt, DABCO, DBU, and TMG. Kinetic traces of the reaction between **3** and excess O$_2$ in the presence of all studied amines (2 equiv) at −35 °C could be fit well to single-exponential eq 1 with similar values of the pseudo-first-order rate constant (Table S15). The rate of oxygenation did not change significantly in the presence of different amines, so no further studies were carried out.
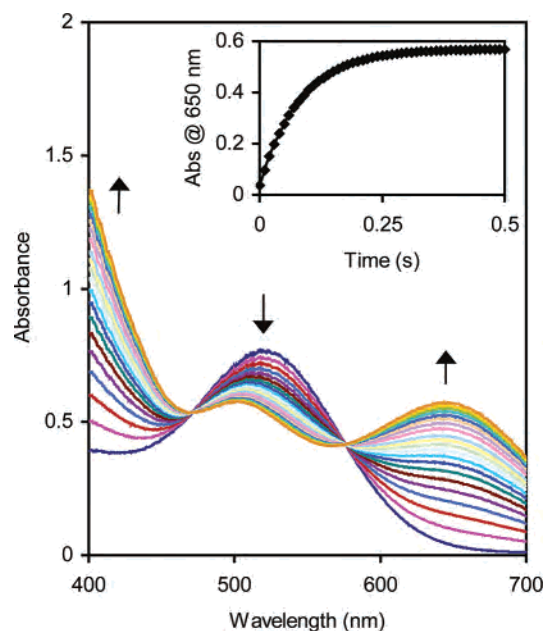

Figure 5. Time-resolved visible spectra acquired by stopped-flow technique during the reaction of complex **4** (0.5 mM) with O$_2$ (4.4 mM) in MeCN at $T = -40$ °C. Inset: kinetic data points superimposed with a pseudo-first-order fit ($k = 12.0$ s^{-1}).

The reaction between complex **3** and excess O$_2$ in acetonitrile was studied by stopped-flow spectrophotometry in the temperature range from −40 °C to −15 °C. The reaction has two stages, which correspond to the formation and decay of the oxygen adduct **3·O$_2$**, respectively. The maximum yield of the **3·O$_2$** intermediate in the course of the reaction is about 35% at −35 °C (Figure S21). The kinetic parameters for the reaction between **3** and O$_2$ in MeCN are very similar to those determined in CH$_2$Cl$_2$ (Table 5).

Addition of amine to the starting solution of complex **3** in acetonitrile significantly improved the yield of peroxo complex **3·O$_2$**. In the presence of triethylamine or DBU (2 equiv) at −35 °C, the yield of **3·O$_2$** was about 70% (Figure S21). The reaction rate was only about 10% slower compared to that in neat MeCN (Table S15), and the activation parameters were not influenced significantly by the addition of amine (Table 5, Figure S22).

Oxygenation of 4. The red-purple complex [Fe$_2$(μ-OH)$_2$-(BnBQA)$_2$(MeCN)$_2$](ClO$_4$)$_2$ (**4**) reacts with O$_2$ in MeCN solution very rapidly at −40 °C forming a dark green dioxygen adduct **4·O$_2$** ($\lambda_{max} = 502$ nm, $\epsilon = 1300$ M^{-1} cm^{-1}; $\lambda_{max} = 650$ nm, $\epsilon = 1300$ M^{-1} cm^{-1}) (Figures 5, S23). Because the solid complex **4** had a limited shelf life, an alternative method of preparing solutions of **4** was developed by mixing monomeric complex **5**(ClO$_4$)$_2$ with 2 equiv of triethylamine in acetonitrile. Kinetics of oxygenation of solutions of **4** prepared from a solid dimeric complex and solutions of **4** generated in situ from **5** and NEt$_3$ were found to be identical. In most kinetic measurements, solutions of **4** generated in situ were used. Kinetic studies at low temperature (−45 to −20 °C) showed that the reaction was first order in each of the reagents (**4** and O$_2$) with a second-order rate constant of 2700 M^{-1} s^{-1} at −40 °C and the

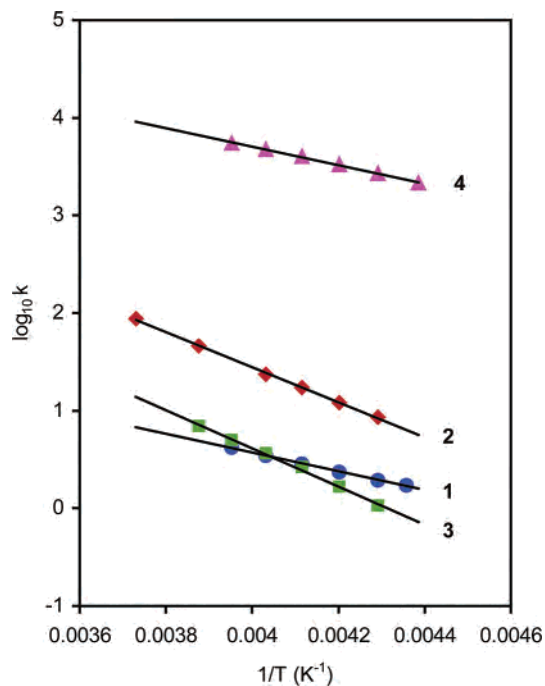**Figure 6.** Arrhenius plots of the second-order rate constants (M^{-1} s^{-1}) for the oxygenation of diiron(II) complexes **1–4** in MeCN at low temperatures (−45 to −5 °C).

activation parameters $\Delta H^{\ddagger} = 16 \pm 2$ kJ mol^{-1} and $\Delta S^{\ddagger} = -108 \pm 10$ J mol^{-1} K^{-1} (Tables S16–S18, Figures S23–S25). The main difference between **4** and the other diiron(II) complexes (**1–3**) is that the oxygenation of **4** proceeds about 3 orders of magnitude faster in MeCN (Figures 5 and 6). Complex **4** dissolves in CH_2Cl_2 with decomposition, and therefore, the oxygenation reaction could not be studied in that solvent. It should be noted that, for other complexes (**1–3**), the change of solvent from MeCN to CH_2Cl_2 did not alter significantly the kinetic parameters of the oxygenation reaction (Table 4).

Discussion

Diiron(II) complexes **1–4** all react with dioxygen. Under carefully selected conditions of solvent and temperature, the oxygenation of complexes **1**, **3**, and **4** yields diiron(III) peroxo species in high yield (Table 4). Under other conditions, the reaction products are oxo-bridged di- or triiron(III) complexes without any observable intermediates. The kinetics of the oxygenation of **1–4** in solution were studied by stopped-flow techniques at low temperatures. In all cases, the reaction is first order in diiron(II) complex and first order in O_2 (second order overall) and characterized by low enthalpies of activation ($\Delta H^{\ddagger}$ from 16 to 36 kJ mol^{-1}) and strongly negative entropies of activation ($\Delta S^{\ddagger}$ from −177 to −80 J mol^{-1} K^{-1}). The values of rate constants and activation parameters of the reactions are compared in Table 5 and Figure 6. For any particular diiron(II) complex (**1–4**), the kinetic parameters do not depend substantially on the solvent and the observable reaction product (peroxo vs oxo-bridged oligoiron(III) complexes). The kinetic data we have obtained suggest that the first and rate-limiting step of the reaction is the association of the diiron(II) complex and O_2 leading to the oxidation of the diiron(II) center.

Scheme 4. Proposed Reaction Pathway of the Oxygenation of Complexes **1–4**
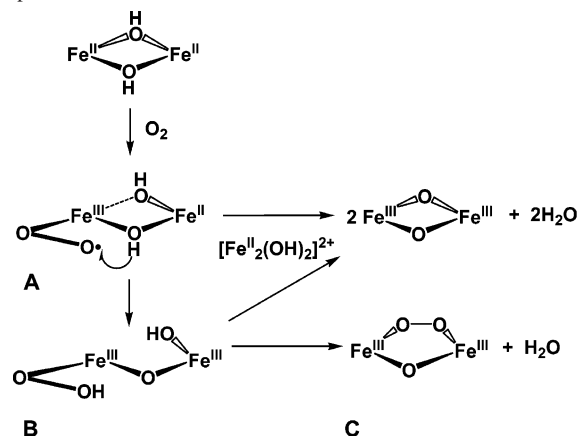
The Rate-Limiting Dioxygen Binding Step. The rate of oxygenation of the diiron(II) complexes increases in the order **1** ∼ **3** < **2** ≪ **4** (Table 5). The initial oxidation of the diiron(II) center may involve either an inner-sphere or outer-sphere process. However, an outer-sphere one-electron transfer would appear to be quite unlikely, because the potential for the O_2/O_2^- redox pair in organic solvents (ca. −1250 mV vs Fc^+/Fc in MeCN and CH_2Cl_2, Table 3)[35,56−59] is about 1 V more negative than those determined for the $Fe^{II}Fe^{III}/Fe^{II}Fe^{II}$ redox pairs for **1–4** (−460 to −150 mV vs Fc^+/Fc, Table 3). Furthermore, there is no correlation between the half-wave redox potentials for **1–4** with the rates of their oxygenation (Table 5). In particular, **3** and **4** exhibit nearly identical redox potentials, but the oxygenation rate of **4** is about 10^3 times faster than that of complex **3**. Thus, an outer-sphere mechanism is highly unlikely.[70]

A more probable mechanism involves the rate-limiting coordination of the O_2 molecule to the diiron(II) center. The trend in the rate constants of the oxygenation reactions (**1** ∼ **3** < **2** ≪ **4**) follows the order of decreasing ligand bulk and increasing access to the diiron core, fully consistent with an inner-sphere mechanism. Such a mechanism is proposed in Scheme 4.

Complex **1** has the slowest rate of oxygenation of the four complexes studied (Table 5). The results reported here for the triflate salt of **1** agree with previous observations on the perchlorate salt,[27] showing that the counterions play no role in the oxygenation reaction. The slow kinetics can be attributed to the 6-methyl substituents of the 6-Me$_3$-TPA ligand that severely restrict access of O_2 to the diiron(II) core,[27] as illustrated by the space filling model shown in Figure 7A. Because of the congestion about the diiron(II) core and the coordinative saturation of the iron(II) ions, it seems highly unlikely that O_2 could coordinate to both iron(II) centers in one step. The O_2 molecule would more likely bind to one metal ion first to form a transient Fe(II)Fe(III)−superoxo species as the first intermediate. Similar intermediates have been proposed for the oxygenation of other diiron(II) complexes[22,27−29] (including MMO[1,7]), but a superoxo intermediate has not yet been characterized. For

---

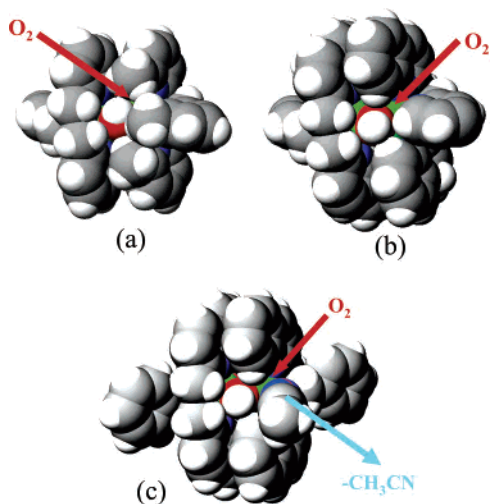(70) Marcus, R. A. *Angew. Chem., Int. Ed. Engl.* **1993**, *32*, 1111−1121.

Figure 7. Space-filling representations of the X-ray structures of the complexes **1** (a), **3** (b), and **4** (c): C, gray; H, white; N, blue; O, red; Fe, green.

1, its superoxo intermediate (**1A**) must then undergo a series of faster transformations to yield the first detected reaction product, the (μ-oxo)(μ-peroxo)diiron(III) intermediate (**1C**), and then a bis(μ-oxo)diiron(III) complex upon thermal decay (Scheme 4).

The first step of the mechanism requires ligand dissociation to make at least one metal center coordinatively unsaturated. Examination of the crystal structure of **1** (Figure 2) identifies two plausible candidates for the dissociable ligand. Complex **1** has an asymmetric Fe$_2$(μ-OH)$_2$ core with one short ($\sim$1.99 Å) and one long ($\sim$2.18 Å) Fe−OH bond based on the structures of **1**(ClO$_4$)$_2$ and **1**(OTf)$_2$ (Table 2). Breaking the weaker Fe−OH bond would cost little energy and could be compensated for by concomitant O$_2$ binding in the transition state. It is also conceivable for one of the pendant pyridine arms to dissociate, as observed for some mononuclear iron(II) complexes of 6-substituted TPA ligands.[71] For **1**, the in-plane Fe−N$_{py}$ bond is quite weak ($\sim$2.30 Å) and could thus dissociate to allow O$_2$ binding. The activation parameters found for O$_2$ binding to **1** (Table 5) support this ligand dissociation scenario: the activation enthalpy (16 kJ mol^{-1}) is relatively small, while the activation entropy is very unfavorable (ca. −170 J mol^{-1} K^{-1}) due to the steric hindrance. These results suggest that oxygenation of diiron(II) complexes may be facilitated by mitigation of the steric bulk from the 6-Me$_3$-TPA ligand to afford a more favorable activation entropy.

At the other extreme of steric bulk is **2**, a complex of the unsubstituted TPA ligand. It reacts with O$_2$ at a rate severalfold faster than **1** in the studied temperature range. An examination of its activation parameters shows that, while there is a favorable change in activation entropy (as expected), this gain is counterbalanced by an unfavorable increase in activation enthalpy (from 16 kJ mol^{-1} for **1** to ca. 31 kJ mol^{-1} for **2**, Table 5). Analysis of the structural data suggests that this increase in activation enthalpy may

(71) Mandon, D.; Machkour, A.; Goetz, S.; Welter, R. *Inorg. Chem.* **2002**, *41*, 5364−5372.

be a result of stronger bonds for the candidate ligands for the dissociation step. Specifically, the Fe$_2$(μ-OH)$_2$ core in **2** is less asymmetric than in **1**, with the weaker Fe−OH bond having a distance of $\sim$2.15 Å for **2**, compared to $\sim$2.18 Å for **1** (Table 2). The in-plane Fe−N$_{py}$ bond of **2** (2.19 Å) is also shorter than that in **1** ($\sim$2.30 Å). Thus, the strengthening of either bond can account for the observed increased activation enthalpy of the oxygenation reaction.

Interestingly, the reaction of **2** with O$_2$ does not result in the observation of a peroxo intermediate. Instead the reaction affords [Fe$^{III}_3$(μ-O)$_3$(TPA)$_3$]$^{3+}$, the more stable oligomer of the presumed initial [Fe$^{III}_2$(μ-O)$_2$(TPA)$_2$]$^{2+}$ product. It is likely that the complete absence of 6-methyl substituents on the pendant pyridines results in a much more exposed diiron core that cannot stabilize a peroxo intermediate.

The ligand BQPA provides a degree of steric shielding around the diiron core that is intermediate between TPA and 6-Me$_3$-TPA. Structural studies of complexes **1**−**3** demonstrated that a 6-substituent on a pyridine ring introduces sufficient steric hindrance in the vicinity of the iron center to cause a lengthening of the Fe−N bond. The BQPA ligand has only two pendant arms with 6-substituted pyridine rings, and these substituents consist of aromatic sp^2 carbons that impose less steric bulk around the metal center than the sp^3-carbon substituents in 6-Me$_3$-TPA. The decrease in steric shielding about the diiron(II) core of **3** relative to that of **1** is evident from the space filling model of the X-ray structure shown in Figure 7B. However, **3** reacts with O$_2$ at rates comparable to **1**. As observed for **2**, there is a favorable change in activation entropy that is counterbalanced by an unfavorable increase in activation enthalpy. Similarly, the candidate ligands for dissociation in **3** have stronger bonds than corresponding ones in **1**; the longer Fe−μ-OH distance is 2.10 Å, and the in-plane Fe−N$_{py}$ distance is 2.17 Å.

Like **2**, **3** reacts with O$_2$ to afford an oxo-bridged diiron(III) complex even at low temperature. However, the peroxo intermediate **3·O$_2$** can be trapped if the oxygenation is carried out in the presence of an added base. Interestingly, the kinetic parameters obtained under the two reaction conditions are essentially identical. This result shows that the oxygen binding step that is probed by the kinetic measurements is the same irrespective of the presence of base and that adding base affects the chemistry after the formation of the initial O$_2$ adduct. (Further discussion on the chemistry associated with the presence of added base can be found in the next section.)

The last complex in our series, **4**, uses the tridentate ligand BnBQA, which is related to the tetradentate BQPA, except for the replacement of the 2-pyridylmethyl pendant arm with a sterically analogous, but noncoordinating, benzyl group. The resulting complex differs from the other bis(μ-hydroxo)-diiron(II) complexes in having a tridentate meridional ligand (BnBQA) and a molecule of coordinated MeCN instead of a tripodal tetradentate ligand (Figures 2 and 7c). Notably, **4** reacts with O$_2$ 3 orders of magnitude faster than **1** in the studied range of temperatures (Figure 6, Table 5), with an activation enthalpy comparable to that of **1** and an activation entropy comparable to those of **2** and **3**. While the alleviation

of congestion around the diiron core readily rationalizes the more favorable activation entropy relative to that of **1**, the comparable activation enthalpies of **1** and **4** suggest that metal−ligand bonds of comparable strength are broken in the rate-determining step. Comparison of the two candidate bonds in **4** suggests that it must be the in-plane Fe−NCMe bond that is broken, as its distance of 2.29 Å is comparable to the ∼2.30 Å distance for the in-plane Fe−N$_{py}$ bond in **1**. In contrast, the weaker Fe−μ-OH bond (2.09 Å) of **4** is significantly shorter than the corresponding bond in **1** (2.18 Å). Thus, both enthalpic and entropic factors accelerate the oxygenation kinetics of **4**. Taken together, the kinetic results for the four complexes strongly suggest that the attack of O$_2$ on the diiron(II) core occurs by displacement of an in-plane nitrogen ligand, rather than the weaker hydroxo bridge in the Fe$_2$(μ-OH)$_2$ core.

Product Determining Steps Subsequent to Dioxygen Binding. The nature of the polydentate ligand also affects the fate of the O$_2$ adduct after the rate-limiting step, affording either the peroxo intermediate or the bis(μ-oxo)diiron(III) complex. The peroxo intermediate is favored by the presence of at least two pendant pyridines with 6-substituents, low temperature, and addition of base in the case of **3**. The steric hindrance introduced by the 6-substituents prolongs the lifetime of the peroxo intermediate at low temperature. However, the effect of added base in the case of **3** suggests a requirement for the loss of a proton to form the peroxo intermediate. It is clear that the added amine affects only the reaction steps after the rate-limiting step, because there are no changes in the UV−vis spectrum of the starting diiron(II) complex or the kinetics of its reaction with O$_2$. The role of the added amine is most probably that of a general base, since DBU and especially TMG acted more efficiently in generating the peroxo intermediate than Et$_3$N, i-Pr$_2$NEt, or DABCO, consistent with the stronger basicities of the former group of amines. There thus appears to be a proton-sensitive branching point after O$_2$ binding that determines the nature of the product.

The mechanism proposed in Scheme 4 can account for these experimental observations. As discussed in detail in the previous section, the rate-limiting step is a bimolecular reaction between the diiron(II) complex and O$_2$ yielding a superoxo Fe(II)Fe(III) species designated **A**, which does not accumulate in the reaction mixture and exists as a steady-state intermediate with a low concentration. The next step is a hydrogen-atom transfer or a proton-coupled electron transfer to form intermediate **B**, which is analogous to that proposed for the formation of oxyhemerythrin after the initial O$_2$ binding step.[72] Loss of H$_2$O then leads to peroxo intermediate **C**. Alternatively, a second equivalent of diiron(II) complex may be oxidized by **A** or **B** to form 2 equiv of the bis(μ-oxo)diiron(III) product. The product is determined by the relative rates of the two steps, with the latter clearly favored at ambient temperature for all four complexes.

There are two possibilities for the base-sensitive species, either the hydroxo bridge in **A** or the coordinated hydro-

peroxide in **B**. Loss of either proton should facilitate formation of a 1,2-peroxo bridge. The pK_a of this proton is determined by the Lewis acidity of the metal center, as modulated by the polydentate ligand. As indicated by its low energy iron(II)-to-pyridine charge transfer band (Figure 1) and rather negative Fe^{II}Fe^{III}/Fe^{II}Fe^{II} redox potential (Table 3), **2** has the least Lewis acidic metal center of the four complexes. The consequent higher pK_a of the hydroxo proton in **A** or the hydroperoxo proton in **B** would disfavor formation of the peroxo intermediate, while the more negative redox potential of the diiron(II) precursor would promote formation of the bis(μ-oxo)diiron(III) product. On the other hand, **1** has the most Lewis acidic metal center, which lowers the pK_a of the hydroxo proton in **A** or the hydroperoxo proton in **B** sufficiently to promote formation of the peroxo intermediate even in the absence of added base. At the same time, its higher redox potential disfavors the bimolecular self-oxidation pathway at low temperature.

Complex **3** represents an intermediate case that allows added base to determine the course of its reaction with O$_2$. In neat CH$_2$Cl$_2$, self-oxidation occurs, but in neat MeCN, the peroxo complex **3·O$_2$** forms in a relatively low yield due to the weakly basic nature of MeCN. Addition of a strong base in either solvent favors formation of the peroxo intermediate.

The clean formation of the peroxo intermediate in the case of **4** suggests that its diiron center is more Lewis acidic than that in **3**. The greater Lewis acidity of the metal center in **4** may be rationalized by the replacement of the pyridine ligand in **3** with the less basic MeCN ligand in **4** and is corroborated by two observations: (a) that the iron(II)-to-quinoline charge transfer band in **3** is red-shifted relative to that of **4** (Figure 1), and (b) that the peroxo-to-iron(III) charge transfer band of **3·O$_2$** is blue-shifted relative to that of **4·O$_2$** (Table 4, Figure 4). Thus, the effect of the 6-substituents on the pyridine ligands is not only steric but also electronic. In addition, peroxo intermediate formation may also be promoted by the facile displacement of MeCN on the second iron, a feature not available for the other complexes.

Summary and Perspective

A series of bis(μ-hydroxo)diiron(II) complexes **1**−**4** with polydentate aminopyridine ligands has been synthesized and structurally characterized. The ligands used in the series (Scheme 2) are tetradentate TPA (**2**), tetradentate BQPA (**3**), and tridentate BnBQA (**4**), and tetradentate 6-Me$_3$TPA (**1**), listed in order of increasing steric congestion around the diiron(II) core as indicated by the number of pyridine ligands with 6-substituents. Electrochemical studies show that this relative order also corresponds to the order of Fe^{III}Fe^{II}/Fe^{II}Fe^{II} redox potentials ranging from −460 to −150 mV versus Fc$^+$/Fc (in MeCN or CH$_2$Cl$_2$), confirming that 6-substituted pyridines favor the iron(II) state.[39] All four complexes react readily with O$_2$ in similar bimolecular associative processes. Interestingly, the three complexes with tetradentate ligands (**1**−**3**) have comparably slow oxygenation rates despite having ligands with different steric requirements. Oxygenation rates of these complexes are constrained by a very

(72) Brunold, T. C.; Solomon, E. I. *J. Am. Chem. Soc.* **1999**, *121*, 8288−8295.

unfavorable activation entropy in the case of **1** due to steric congestion around the diiron core and by relatively large activation enthalpies for less hindered complexes **2** and **3** arising from the required dissociation of a more strongly bound ligand in the rate-limiting step. In contrast, the complex with the tridentate ligand (**4**) reacts with O$_2$ much faster. The use of tridentate BnBQA introduces MeCN as the sixth ligand on each iron in place of the third arm of the tetradentate ligands, and its kinetic lability lowers the activation enthalpy for oxygenation. At the same time, the reduced steric crowding around the diiron core of **4** also makes the activation entropy less unfavorable. So enthalpic and entropic factors combine to give rise to the 1000-fold rate acceleration observed for **4**.

The remarkable effect of added base in promoting peroxo intermediate formation in the case of **3** has revealed the involvement of a proton-sensitive step that controls the fate of the initial O$_2$ adduct **A** (Scheme 4). In the absence of base, O$_2$ adduct **3A** or its isomer **3B** can oxidize residual **3**. Interestingly, **3·O$_2$** does not react with added **3**; neither do **1·O$_2$** and **4·O$_2$** with their respective diiron(II) precursors. These results suggest that the (μ-1,2-peroxo)diiron(III) state is relatively unreactive and thus may not be directly involved in oxidation reactions. This relative stability may account for the fact that almost all O$_2$ adducts of synthetic diiron centers have been characterized to be (μ-1,2-peroxo)-diiron(III) complexes.[73] Indeed, the oxidative reactivities of synthetic (μ-1,2-peroxo)diiron(III) intermediates[24,28,29] and related systems[74] investigated so far are generally poor; they only work on easily oxidizable functional groups and often require substrate coordination to the metal center.

Dioxygen adducts of diiron enzymes are also characterized to have (μ-1,2-peroxo)diiron(III) centers such as those found for D84E RNR R2[75] and chemically reduced Δ9D desaturase;[9] these intermediates are also quite stable and similarly unreactive. However, it has been demonstrated that the conversion of diiron(III)−peroxo intermediate MMO-**P** to methane oxidizing diiron(IV) intermediate MMO-**Q** requires a proton.[76] So protonation of the (μ-1,2-peroxo)diiron(III) intermediate **C** (Scheme 4) may be required to activate the O−O bond for cleavage in order to attack aliphatic C−H bonds such as those oxidized by methane monooxygenase and fatty acid desaturases. This protonation strategy is utilized by heme enzymes to promote cleavage of the O−O bond.[77−79] Efforts to trap an HOO−Fe^{III}−O−Fe^{III} intermediate (species **B** of Scheme 4) and characterize its reactivity are ongoing.

Supporting Information Available: Crystallographic data in CIF format and additional figures and tables. This material is available free of charge via the Internet at http://pubs.acs.org.

IC0485312

(73) Girerd, J.-J.; Banse, F.; Simaan, A. J. *Struct. Bonding* **2000**, *97*.
(74) Carson, E. C.; Lippard, S. J. *J. Am. Chem. Soc.* **2004**, *126*, 3412−3413.
(75) Voegtli, W. C.; Khidekel, N.; Baldwin, J.; Ley, B. A.; Bollinger, J. M., Jr.; Rosenzweig, A. C. *J. Am. Chem. Soc.* **2000**, *122*, 3255−3261.
(76) Lee, S.-K.; Lipscomb, J. D. *Biochemistry* **1999**, *38*, 4423−4432.
(77) Sono, M.; Roach, M. P.; Coulter, E. D.; Dawson, J. H. *Chem. Rev.* **1996**, *96*, 2841−2888.
(78) Harris, D. L.; Loew, G. H. *J. Am. Chem. Soc.* **1998**, *120*, 8941−8948.
(79) Loew, G. H.; Harris, D. L. *Chem. Rev.* **2000**, *100*, 407−420.